Geochemistry and isotopic evolution of the central African Domes, Bangweulu and Irumide regions: evidence for cryptic Archean sources and a Paleoproterozoic continental arc

David Debruyne, Jorik Van Wilderode, Lieve Balcaen, Frank Vanhaecke, Philippe Muchez

PII: S1464-343X(14)00192-7
DOI: http://dx.doi.org/10.1016/j.jafrearsci.2014.06.013
Reference: AES 2078

To appear in: *African Earth Sciences*

Received Date: 23 April 2014
Revised Date: 16 June 2014
Accepted Date: 17 June 2014

Please cite this article as: Debruyne, D., Wilderode, J.V., Balcaen, L., Vanhaecke, F., Muchez, P., Geochemistry and isotopic evolution of the central African Domes, Bangweulu and Irumide regions: evidence for cryptic Archean sources and a Paleoproterozoic continental arc, *African Earth Sciences* (2014), doi: http://dx.doi.org/10.1016/j.jafrearsci.2014.06.013

Geochemistry and isotopic evolution of the central African Domes, Bangweulu and Irumide regions: evidence for cryptic Archean sources and a Paleoproterozoic continental arc.

David Debruyne[a,*], Jorik Van Wilderode[a], Lieve Balcaen[b], Frank Vanhaecke[b], Philippe Muchez[a]

[a] KU Leuven, Department of Earth and Environmental Sciences, Celestijnenlaan 200E B-3000 Leuven, Belgium

[b] Ghent University, Department of Analytical Chemistry, Ghent University, Krijgslaan 281-S12, B-9000 Ghent, Belgium

[*] **Corresponding author**: Tel: +32 497 16 58 69; email: david.debruyne@ees.kuleuven.be

Abstract

The interregional cratonic relations between the Paleo- and Mesoproterozoic basement units surrounding the Neoproterozoic Central African Copperbelt are still largely unresolved, although they are regarded as major potential metal sources. This study focuses on the Domes region basement at depth below the Copperbelt and its relationship to the neighboring Bangweulu Block and its destabilized margin, the Irumide Belt. We applied an integrated whole rock petrochemical and Sm-Nd isotopic approach to major lithological units to assess the proposed mid-Proterozoic arc setting for the Domes basement inliers along with their relationship to the neighboring areas. The available petrochemical and isotopic data for the Paleoproterozoic eastern Domes granitoids and magmatic units in the SW Bangweulu Block is consistent with a continental arc setting. Moreover, the mid-Paleoproterozoic Nd isotope ratios preclude an island arc because they are significantly less radiogenic than the depleted mantle. Predominantly Archean and Early Paleoproterozoic depleted mantle model ages in all terranes indicate limited juvenile input during Paleo- and Mesoproterozoic magmatic phases. Finally, broadly similar model ages in the Domes inliers and the Bangweulu-Irumide region suggest a relationship between these terranes.

Keywords: Chemistry; Sm-Nd; Nd model age; Arc terrane; Granite; Metasediments

1. Introduction

The Central African Copperbelt is one of the world's largest Copper provinces (e.g., Cailteux et al., 2005). The basement units surrounding the Neoproterozoic Copperbelt are seen as major potential copper and cobalt sources for this stratiform Cu-Co province (e.g., Cailteux et al., 2005; Sweeney et al., 1991; Van Wilderode et al., 2014). The Paleoproterozoic Domes inliers lie directly below the Copperbelt deposits, yet their Paleo- to Mesoproterozoic history and the relation with the neighboring basement units is still largely unknown. A few occurrences of inherited Meso- to Neoarchean xenocrystic zircons in the Domes region suggest that these inliers rework a cryptic Archean terrane (De Waele et al., 2006b; Rainaud et al., 2002, 2003). This was recently confirmed by zircon εHf depleted mantle model ages (Eglinger, 2013). Because the Bangweulu Block and its southeastern destabilized margin, the Irumide Belt, also rework Archean crustal sources (e.g., De Waele et al., 2006b), these inliers could represent the western destabilized margin of the Bangweulu Block (Eglinger, 2013). Various authors suggested that the Domes inliers were part of an extensive arc terrane system between c. 2050 Ma and c. 1850 Ma, stretching either to the Ubendian Belt (Brewer et al., 1979; Kabengele et al., 1991) or towards Namibia (Rainaud et al., 2005). Zircon U-Pb dating by Eglinger (2013) indicated a metamorphic episode in the Domes region at 1190-1150 Ma. However, this cannot be used as an argument for a relationship with the Irumide Belt as it predates the Irumide Orogeny that culminates at ~1020 Ma (De Waele et al., 2006b).

A combined petrochemical and isotopic approach has been used to determine the relationship between the Domes inliers and two neighboring basement units, the Bangweulu Block and the Irumide Belt. Depleted mantle Nd model ages for major basement lithologies were used to estimate crustal residence times which were compared between the basement units. This isotopic approach was combined with a petrochemical characterization to compare the geotectonic setting of contemporaneous magmatic phases across the basement units.

We will demonstrate that careful use of whole rock (isotope) data in conjunction with the available temporal framework can provide insights in interregional cratonic relations and geotectonic history of

Proterozoic basement units. Moreover, the whole rock isotopic approach allows to determine whether the isotopic differences are sufficient to act as source tracers for base metal mineralizations.

2. Geological setting

2.1 Bangweulu Block

The Bangweulu Block is a Paleoproterozoic cratonic region of 275 by 450 km, surrounded by orogenic belts (Fig. 1; e.g., Andersen and Unrug, 1984). To the north, the Paleoproterozoic Ubendian and Usagaran Belts separate it from the Archean Tanzania Craton, whereas the Mesoproterozoic Kibara Belt and the Neoproterozoic Lufilian Foreland separate it from the Kasai Shield in the west (e.g., De Waele et al., 2008). The Mesoproterozoic Irumide Belt located to the southeast of the Bangweulu Block was recently identified as a destabilized (metacratonized) margin of the Bangweulu Block (De Waele et al., 2006b). Such metacratonic margins are generated by attempted subduction of a passive continental margin, resulting in a partial loss of their cratonic rigidity and increasing their susceptibility to magmatism during subsequent deformation (e.g., Black and Liégeois, 1993; Adbelsalam et al., 2002; Liégeois et al., 2013).

Initial destabilization of the southern part of the Bangweulu craton occurred during the Paleoproterozoic when an unknown terrane collided with the Irumide margin. This collision resulted in voluminous magmatism throughout the Bangweulu region at 2050-1930 Ma, and this event represents the most recent major magmatic event recorded in this area (De Waele et al., 2006b). The crystalline Bangweulu basement consists of E-W oriented schist belts intruded by granitoids and overlain by metavolcanic rocks. The schist belts occur mainly in the eastern and northeastern parts of the Bangweulu Block as E-W oriented rafts which are up to 10 km wide and 75-100 km long (Andersen and Unrug, 1984). Farther south, the schist belts are less extensive and occur as discrete rafts (Andersen and Unrug, 1984). In the central part of the Bangweulu Block, the schist belts are weakly metamorphosed, dominated by assemblages of chlorite, muscovite and biotite schists associated with quartzites. These rafts either terminate against major shear zones or grade into higher grade equivalents in the Ubendian Belt, indicating a relationship between the Bangweulu and this belt (Andersen and Unrug, 1984; De Waele et al., 2006b). Towards the Ubendian Belt, sillimanite- and

cordierite-bearing gneisses and migmatites indicate higher metamorphic grades, and the structural trends are oriented NNW-SSE, parallel to the Ubendian Belt (De Waele et al., 2006b). The relatively undeformed Bangweulu granitoids are interpreted as shallow intrusions because they are associated with volcanic rocks (e.g., Brewer et al., 1979; Schandelmeier, 1980, 1983). The coeval volcaniclastic rocks are andesitic to rhyolitic in composition and are dominantly pyroclastic with subordinate lava flows and shallow intrusions (Brewer et al., 1979). Andersen and Unrug (1984) interpreted these as forming in a volcanic arc system situated along an active margin because the granitoids and the coeval volcanics display high-K calcalkaline compositions. Due to the absence of indications for significant crustal thickening and subsequent unroofing in the Bangweulu Block, these granitic rocks and the associated metavolcanic rocks were possibly generated in an intracontinental setting (De Waele et al., 2006b).

The Paleo- to Mesoproterozoic sedimentary cover of the Bangweulu Block also stretches out over parts of the Irumide and Domes regions. This cover is collectively termed the Muva Supergroup and comprises undeformed units in the north and strongly deformed units in the Irumide Belt (De Waele et al., 2005; De Waele and Fitzsimons, 2007). In the Bangweulu Block, it comprises the Mporokoso Group in the northwest and the Kasama Formation, a minor unit exposed in an E-W oriented basin to the east of the Mporokoso Group. The Mporokoso Group contains fluvial and lacustrine sediments, with minor aeolian sediments with a southern sediment source (Andersen and Unrug, 1984) and has a maximum depositional age of 1829 ± 19 Ma constrained by detrital zircons (De Waele and Fitzsimons, 2007). Based on paleocurrent analysis, the extreme maturity of the Kasama quartzites and arenites, and on age modes of detrital zircons, they are interpreted as a reworking of the Mporokoso Group sediments to the west (Andersen and Unrug, 1984; De Waele and Fitzsimons, 2007). The depositional age of the Kasama Formation is constrained by detrital zircons and an Irumide-aged deformation between c. 1434 and 1020 Ma (De Waele and Fitzsimons, 2007). The Muva Supergroup is in turn overlain by Neoproterozoic Katanga Supergroup sediments and Cenozoic fluviatile and lacustrine sediments which are not discussed here (Andersen and Unrug, 1984).

2.2 Irumide Belt

The Irumide Belt is characterized by voluminous Mesoproterozoic K-feldspar porphyric granitoids and strongly deformed and metamorphosed supracrustal sequences coexisting with Paleoproterozoic granitoids and minor Neoarchean granitic rocks (Fig. 1; De Waele et al., 2006b). Extensive studies by De Waele et al. (2001, 2005, 2006a, 2006b, 2009) indicate that the Irumide region was a passive margin to the Bangweulu Block during most of the Paleo- and Mesoproterozoic which was destabilized to form a metacraton.

Initial metacratonization in the Irumide Belt occurred at 2050-1930 Ma and involved continental collision with an unidentified block approaching from the present-day south, resulting in the formation of the Usagaran Belt and magmatism throughout the Irumide and Bangweulu regions (De Waele et al., 2006b). This collision was associated with dextral transpression, dominantly vertical plate movements and resulted in magmatism and brief, but potentially deep, subduction accompanied by eclogite-grade metamorphism (De Waele et al., 2006b).

Deposition of the Muva Supergroup molasse occurred simultaneously and renewed convergence generated the Ubendian Belt at 1880-1850 Ma, after which deposition of the Muva Supergroup continued in a passive margin setting (De Waele et al., 2006b). This was followed by a period of relative quiescence, until minor reactivation at 1660-1550 Ma generated the anorogenic granites of the Lukamfwa phase (De Waele et al., 2006b). Between ~1080 and 1050 Ma, convergence of the Irumide with an unknown terrane and southward subduction resulted in continental arc magmatism in a part of this terrane now known as the Southern Irumide Belt (De Waele et al., 2006b; Johnson and Olivier, 2004; Johnson et al., 2005, 2006; 2007b).

The subsequent collision resulted in the Irumide Orogeny at 1050-1000 Ma and generated voluminous K-feldspar porphyric granitoids which are restricted to the Irumide Belt. Finally, post-orogenic collapse was associated with minor A-type magmatism around 950 Ma (De Waele et al., 2006b). Bimodal magmatism of c. 880 Ma is interpreted as a rift event which removed part of the colliding terrane, leaving the Southern Irumide Belt behind (De Waele et al., 2006b; Johnson et al., 2006; 2007b). The Karoo Graben which developed along the Proterozoic Mwembeshi Shear zone currently separates the Irumide from the Southern Irumide Belt. This graben likely reactivated the suture

between these belts, represented by a SE-declining paleo-Benioff zone marking the northern margin of the Southern Irumide Belt (De Waele et al., 2006b; Johnson et al., 2006; 2007b).

In the Irumide Belt, the Muva Supergroup includes the Kanona, Manshya River and Mafingi Groups (e.g., De Waele and Fitzsimons, 2007). The Mafingi Group occurs in the NE end of the Irumide Belt, has a limited extent and was correlated with the Manshya River Group in the northeastern part of the Irumide Belt (e.g., De Waele and Fitzsimons, 2007; Fitches, 1971). The depositional age of the Manshya River Group is constrained by conformal rhyolites dated at 1880 ± 12 Ma (De Waele and Mapani, 2002).

The Kanona Group comprises extensively deformed supracrustal sequences occurring in the SW Irumide Belt and consists of mature quartzites and pelitic rocks (De Waele and Mapani, 2002). Based on broad similarities in lithostratigraphy, the Manshya River and Kanona Group sedimentary rocks are inferred to be coeval sequences deposited around 1850 Ma, although direct correlation is impossible due to lack of age constraints and exposure gaps (De Waele and Fitzsimons, 2007; De Waele and Mapani, 2002). These sequences are interpreted as extensive Paleoproterozoic beach deposits with a sediment source to the northwest, deposited in the Irumide Basin that formed after the Ubendian deformation phase (Andersen and Unrug, 1984; De Waele et al., 2001). The absence of carbonates and obducted oceanic crust in the Irumide Belt likely indicates that this was a shallow intracontinental basin (Daly, 1986).

2.3 The Domes Inliers

In the Domes region, basement inliers are exposed within the Neoproterozoic Lufilian Belt. From east to west, the major inliers are the Kafue Basement Complex and the Luswishi, Solwezi, Mwombezhi and Kabompo Domes (Fig. 1). Radiometric age dating of rocks within these inliers indicates mostly Paleoproterozoic ages of 1970-1850 Ma (Eglinger, 2013; John, 2001; Nyogi et al., 1991; Rainaud et al., 2002, 2005). About half of the basement consists of the Lufubu Schist sequence, which is intruded by extensive granitic rocks (Mendelsohn, 1961, Rainaud et al., 2005). The Paleoproterozoic Lufubu Schists in the Kafue Basement Complex comprises mainly schist, quartzite and gneiss with minor metacarbonate, metagreywacke, arkose and conglomerate (Mendelsohn, 1961). The U-Pb ages for

igneous zircons within the Lufubu Schists units cluster around 1980-1960 Ma and 1870-1860 Ma (Rainaud et al., 2005). Mendelsohn (1961) interpreted the Lufubu Schist as a metasedimentary sequence with minor intercalated metavolcanitic rocks. However, Rainaud et al. (2005) argue in favor of a significant proportion of metavolcanic units, mainly based on blastoporphyric textures, occurrence of hornblende and predominantly oscillatory zoned zircons in the Lufubu Schist samples. Many lithologies within the Lufubu Schist are spatially associated with (sub)contemporaneous granitic rocks (e.g., Lobo-Guerrero Sanz, 2005; Rainaud et al., 2005). Based on this association, Rainaud et al. (2005) suggested that the metavolcanic Lufubu Schists and their plutonic contemporaries represent one or several magmatic arc terranes, active between the ~ 2049 Ma age of the Mkushi Gneiss in the Irumide Belt and the youngest Lufubu Schist crystallization age at ~ 1850 Ma. De Waele et al. (2006b) relate the Mkushi Gneiss to the 2050-1930 Ma Usagaran magmatism in a collisional setting between the Irumide Belt and an unidentified terrane. Parts of this complex experienced magmatic reworking in the Mesoproterozoic at 1090 ± 160 Ma (De Waele et al., 2006b; De Waele and Mapani, 2002; Rainaud et al., 2002).

The ~1880 Ma granitoids and volcanic units in the Luina Dome (Ngoyi et al., 1991; Rainaud et al. 2002) are thought to be related to similar, contemporaneous magmatic units in the SW Bangweulu and in the Usagaran Belt (De Waele et al., 2006b). Additionally, combination of zircon U-Pb and εHf data with geothermobarometric data suggests that the Domes inliers represent the southwestern metacratonic margin of the Bangweulu Block, in analogy with the Irumide Belt (Eglinger, 2013). Irumide-aged magmatic events around 1020 Ma are unknown in the Domes region. Nonetheless, recently dated zircon overgrowths revealed a Mesoproterozoic metamorphic event at 1190-1150 Ma in the Mwombezhi Dome and at 1240-1120 Ma in the Solwezi Dome (Eglinger, 2013).

The most recent igneous event in the Domes region inliers is represented by volumetrically minor anorogenic granites such as the 877 ±11 Ma Nchanga granite in the Kafue Basement Complex , thought to be related to incipient rifting (Armstrong et al., 2005; Katongo et al., 2004). Contemporaneous magmatism also occurs in the Southern Irumide Belt, about 400 km southwards from this location, where it has been linked to the earliest breakup phases of the Rodinia Supercontinent (Johnson et al., 2007a).

During the Lufilian Orogeny from c. 595 to 490 Ma (e.g., Selley et al., 2005), the Mwombezhi basement was thrusted on top of the overlaying Neoproterozoic Katanga Supergroup sediments, resulting in a tectonic interlayering (e.g., Cosi et al., 1992). Recent mapping and drilling by Equinox, now part of Barrick Gold, confirmed that the undifferentiated Mwombezhi gneisses are rimmed by tectonic mélanges of basement and Katanga sequence (Bernau, 2007).

3. Methodology

3.1 Sample selection

A set of lithologies was collected that characterize the main suite of exposed granitic and metasedimentary rocks and complement the existing published dataset (e.g., De Waele et al., 2006b; Katongo et al., 2004). Provenance studies indicate that the Kibara Belt did not contribute significant components to the Neoproterozoic Katanga sediments in the Copperbelt and that the Bangweulu Block is likely the dominant sediment source (Shuh et al., 2012). Sampling here has focused on the Domes, Bangweulu and Irumide regions. In the Domes region, 21 samples were collected from the Mwombezhi Dome and the Kafue Basement Complex area (Fig. 1). Samples from two deep Mwombezhi drill cores were kindly provided by Equinox Resources Ltd. These were supplemented by well-located samples from key units within the Kafue Basement Complex in the east, provided by the Royal Museum for Central Africa (RMCA) in Tervuren, Belgium. The samples from the Bangweulu (n=18) and the Irumide (n=14) regions bordering the Copperbelt were collected in a field campaign during 2012. A study by De Waele et al. (2006b) describes mainly felsic igneous units within the Irumide Belt and southern Bangweulu Block in terms of geochemistry, radiometric data, and Rb-Sr and Sm-Nd isotope systems. Special attention was given to metasedimentary and additional mafic rocks to complement this data.

Please insert supplementary Table A here.

3.2 Major and trace element composition

Major and minor elements were measured with a Varian 720 ICP-OES instrument after Li-metaborate fusion. The results are given in Table 1 along with the instrumental detection limits (IDL) calculated from repeated analyses of procedural blanks. For trace element analysis, samples from the Domes, Irumide and Bangweulu regions were dissolved using a microwave-assisted HF-HNO_3-$HClO_4$ digestion adapted from Mareels (2004). After an initial two-phase digestion step at 180 and 200 °C using 6 ml 22 M HF and 2 ml 14 M HNO_3, Re and In were added as internal standards. Fluor was subsequently removed using a near-total evaporation step with 2 ml $HClO_4$, and the resulting droplet was dissolved in 2 ml 14 M HNO_3 at 120°C and diluted to 50 ml with a 2% HCl solution. Trace elements were measured with a Perkin-Elmer SCIEX Elan DRC Plus single collector inductively coupled plasma mass spectrometer (ICP-MS) instrument at Ghent University. Blank subtraction was done with three procedure blanks and calibration is performed with international rock reference standards BCR-1, GA, AGV-1, AWI, NIM-G and GSP-1. Standard solutions were added to the measuring sequence and allowed for internal data quality checks along with duplicate analyses. The results are added in Table 1, along with their respective IDLs. Because many samples have experienced high-grade metamorphism, the geochemical interpretations are mainly based on the immobile trace element content. However, an overview of the present-day major element composition is shown in Figure 2 with quartz alkalifeldspar plagioclase (QAP) diagrams and graphs plotting the aluminum saturation index (A/CNK= molar Al_2O_3 / (Na_2O + CaO + K_2O)) versus the agpaitic index (A/NK = molar Al_2O_3 /(Na_2O +K_2O)).

3.3 Strontium isotope analysis

Powdered rock samples of c. 100 mg were digested on a hot plate using 22 M HF and 14 M HNO_3 in a 3:1 ratio at 120°C in a first step, followed by an aqua regia step with 6 M HCl and 14 M HNO_3. Sr was isolated using Eichrom Sr Spec resin according to the procedure of De Muynck et al. (2009). $^{87}Sr/^{86}Sr$ ratios were determined using a Thermo Scientific NEPTUNE multi-collector (MC) ICP-MS operated in static multi-collection mode and normalized to the invariant $^{86}Sr/^{88}Sr$ ratio of 0.1194. The results from NIST SRM 987 reference standard were in excellent agreement with the $^{87}Sr/^{86}Sr$ ratio from Thirlwall (1991) and procedural blank signals were negligible. Rb and Sr concentrations were

determined using a Thermo Scientific ELEMENT XR single-collector sector field–ICP-MS. The Rb-Sr data is included in the appendix (Table B), because this system was likely reset for many high-grade metamorphic rocks.

3.4 Neodymium isotopic analysis

After using the digestion method described in the previous section, Nd was isolated using two columns containing Eichrom TRU Spec and Ln Spec resins according to procedures developed by Pin et al. (1994) and Ganio et al. (2012). The Nd isotopic composition was determined using a Thermo Scientific NEPTUNE MC-ICP-MS instrument operated in static multi-collection mode. All Nd isotope ratios were normalized to $^{146}Nd/^{144}Nd = 0.7219$. Repeated measurements of the JNdi-1 reference material yielded values in excellent agreement with the accepted value from Tanaka et al. (2000) and procedural blank signals were negligible.

3.5 Depleted mantle Neodymium model ages and uncertainties

Depleted mantle Nd model ages are calculated following the method of Nelson and DePaolo (1985) and represent approximate fractionation ages from the depleted mantle. If there are multiple episodes of juvenile material addition, these ages represent a weighted average of mantle fractionation times (e.g., Farmer and DePaolo, 1983). Equating the sample and depleted mantle evolution lines results in a quadratic equation of the form $aT^2 + bT + c = 0$. The model age T_{DM} (in Ga) then corresponds to the lower intercept with the horizontal axis:

$$0.25T^2 + (-3 + 25.13(\frac{^{147}Sm/^{144}Nd_{\text{sample}}}{0.1964} - 1))T + 8.5 - \varepsilon Nd_{now} = 0$$

Nelson and DePaolo (1985) demonstrated graphically that the uncertainty on this age depends on the proximity to the chondrite $^{147}Sm/^{144}Nd$. The errors induced by the uncertainty on $^{147}Sm/^{144}Nd$ and $^{143}Nd/^{144}Nd$ can be calculated by applying the error propagation equation to the solution for T_{DM} (e.g., Bevington and Robinson, 1992):

$$e(T_{DM})^2 = e(\frac{-2c}{b - \sqrt{b^2 - 4ac}})^2 = e_b{}^2(\frac{2c}{b(b - \sqrt{b^2 - 4ac})) - 4ac})^2 + e_{\varepsilon Nd}{}^2(\frac{1}{\sqrt{b^2 - 4ac}})^2$$

The standard deviation on the present-day εNd_{CHUR} is around 0.5, and is assumed to be uncorrelated with the error on the $^{147}Sm/^{144}Nd$ ratio. The precision on the $^{147}Sm/^{144}Nd$ ratio obtained from section 3.2 is estimated at around 2 % from repeated analyses of the international rock reference standard AGV-1. The analytical uncertainties typically induce model age uncertainties of about 50 to 150 Ma, but this can be much larger for samples with perichrondritic $^{147}Sm/^{144}Nd$ ratios (Table 2). This indicates that the effect of analytical factors are at least equally important as the uncertainty introduced by Sm-Nd fractionation during intracrustal anatexis, estimated at around 100 Ma (Nelson and DePaolo, 1985). All model ages are reported in Ga, following literature conventions (e.g., Nelson and DePaolo, 1985) and to avoid confusion with the radiometric ages from literature, reported in Ma.

4. Results

4.1 Domes region

4.1.1 The western Domes region: Mwombezhi Dome

The drill core from Lumwana (DO01-DO07) and Chimiwungo prospect (DO08-DO13) in the Mwombezhi basement mainly consists of medium to coarse-grained gneiss and migmatite, intercalated with minor amphibolite and biotite-rich schistose layers (Fig 3A, B). The schists contain percentage-levels of chalcopyrite and pyrite. Most gneisses are monzogranitic in composition, with minor granodiorite and quartz monzogabbro compositions (Fig. 2A). The Lumwana and Chimiwungo gneisses contain intermediate to high silica contents between 69 and 75 wt. % SiO_2 and intermediate to high Al_2O_3 between 13.7 and 15.7 wt. %. $Fe_2O_{3(T)}$ ranges from 0.58 to 3.44 wt. % and the CaO, Na_2O and K_2O content ranges between 0.68-2.37, 3.06-5.65 and 1.98-6.79 wt. % respectively. The schistose units contain low to intermediate silica contents and high alumina contents of 54.4-67.6 and 14.1-18.6 wt. % respectively. Their $Fe_2O_{3(T)}$ ranges from 3.93 to 8.16 wt. % while their CaO, Na_2O and K_2O content ranges between 1.30-3.44, 2.60-5.26 and 3.00-6.83 wt. % respectively. The Mwombezhi gneisses are exclusively subalkalic and straddle the border between metaluminous and peraluminous compositions, while the schistose intervals are strongly peraluminous (Fig. 2B). The white Lumwana gneisses are generally slightly peraluminous, with high Mg-numbers between 37 and 48. They are

depleted in rare earth elements (REE) and high field strength elements (HFSE), with low Y/Nb ratios between 0.6 and 1.2. In contrast, the pinkish Chimiwungo prospect gneisses and one pink Lumwana biotite gneiss DO07 are elevated in REE and HFSE, with Y/Nb ratios between 2.8 and 13 (Fig. 4A, 5A). They are either slightly metaluminous with low magnesium-numbers (#25) or strongly peraluminous and biotite-rich with higher magnesium-numbers comparable to the Lumwana samples (Fig. 2B). Because of their low HFSE and REE content, the Lumwana gneisses plot in the volcanic arc or syncollisional granite field in the Nb-Y discrimination diagram (Fig. 6A). Figure 7 shows that the present-day εNd composition of the Mwombezhi basement falls between -20.5 and -18.5 for both the schistose units and the gneisses. Their T_{DM} model ages mostly range between 2.4 and 2.8 Ga, with one older age at c. 3.1 Ga. The basement sequence also contains minor intervals of amphibolites, here represented by amphibolite DO01, which consists dominantly of hornblende, feldspars and biotite, with minor titanite and accessory zircon, magnetite and ilmenite (Fig. 3A). The amphibolite is silica poor, CaO- and Ti_2O-rich, with 46.2, 9.54 and 1.99 wt. % respectively. It has a Mg number of 52, an elevated Ti/V ratio of 42 and La/Yb_{UCC} and Gd/Yb_{UCC} ratios of 0.37 and 1.24 respectively. In figure 4C, the amphibolite shows minor negative Ba, Sr, Ti, Nb and Ta anomalies. It has a present-day εNd of -13 and gives a T_{DM} model age of 2.43 Ga. The Lumwana East Granite (LEG) at the top of the Chimiwungo drill core is a fine-grained, foliated biotite-muscovite monzogranite with sericitized feldspars and accessory allanite and hematite. The LEG is currently alumina-poor and silica-rich with 11.6 wt. % Al_2O_3 and 80 wt. % SiO_2. It is poor in ferromagnesic elements, has a low Zr and Nb content of 105 and 17 ppm respectively and a low U /Th ratio of 0.04. Additionally, it is poor in alkali earths (Ca, Sr, Ba) and has an intermediate to high Na, K and Rb content. This monzogranite is strongly enriched in light REE (LREE), with a pronounced negative Ce-anomaly and high total REE concentrations amounting to 1330 ppm ∑REE (Fig 5B). Its present-day εNd of -25 is lower than those of the Mwombezhi gneisses, yet its Sm/Nd ratio is also much lower. This results in a younger T_{DM} model age of c. 1.93 Ga.

4.1.2 The eastern Domes region: Kafue Basement Complex and Luina Dome

The Kafue Basement Complex is named after the Kafue Anticline, a structure generated during the Lufilian Orogeny (e.g., Porada and Berhorst, 2000), not to be confused with the Kafue town area c. 400 km southwards in the Southern Irumide Belt (e.g., Johnson et al., 2007a). The Mufulira Grey Granite DO18, located within this Basement Complex, is a titanite-rich biotite-epidote granodiorite containing accessory muscovite, magnetite and ilmenite (Fig. 3E). This weakly metaluminous granite contains an intermediate 66.4 wt. % silica and high TiO_2, Fe_2O_3 and CaO contents at 0.72, 5.16 and 3.50 wt. % respectively (Fig. 2A, B). It is strongly sodic with a molar K/Na ratio of 0.65 and a K_2O and Na_2O content around 3.50 wt. %.

The Tshinsenda granitoid rocks DO14 and DO15 in the Luina Dome to the north of the Kafue Basement Complex are titanite-rich feldspar- porphyric biotite-epidote monzogranites with sericitized feldspars and contain accessory zircon and ilmenite (Fig. 3C). Their major element composition is similar to the Mufulira Granite, except that these granitoids are potassic (K/Na ~1.2) and slightly peraluminous. In the Mufulira Grey and the Tshinsenda Granites, opaques are occasionally rimmed by white mica (Fig. 3C, E).

The REEY and spidergram patterns in the Mufulira grey Granite and the Tshinsenda Granite are also similar, with Upper Continental Crust (UCC)-normalized HREE/LREE ratios above unity and pronounced positive Eu- anomalies (Fig. 4B, Fig. 5B). Their UCC-like REEY patterns and relatively low HFSE contents suggest an affinity with syncollisional or arc granites (Fig. 6A). The Mufulira Grey Granite has a present-day εNd of -28, and it gives a model age of 2.49 Ga (Fig. 7). An intrusive contact indicates that this granite postdates the 1994 ±7 Ma Mufulira Pink Granite (U-Pb zircon; Rainaud et al., 2005). The only available age estimate is a c. 1950 Ma Rb-Sr cooling age (Cahen et al., 1970). Based on this estimated age, it gives an εNd(T) composition of -4. The Lufubu Schist samples have similar age-corrected εNd values around 1950 Ma and these have been found as xenoliths in the Mufulira Grey Granite (Brandt et al., 1961). The Tshinsenda Granitic rocks have present-day εNd compositions of -19 and -21 and give model ages of 2.57 and 2.40 Ga (Fig. 7).

Mufulira Lufubu Schist DO19 is an equigranular biotite-chlorite-tourmaline schist, while DO20 is an equigranular quartz-feldspar-chlorite siltstone (Fig. 3F). The Nkana Lufubu Schist NSD49 contains mm-sized, mostly anhedral quartz and (sericitized) feldspar clasts in a fine-grained chlorite-white mica

matrix of about 50 vol. %. In addition, it contains minor green biotite and dolomite cement, along with accessory porphyroblastic cordierite. Quartz often forms elongated polycrystalline aggregates, aligned along the cleavage direction. The Nkana Lufubu Schist also contains an elevated Co content of 186 ppm compared to <9 ppm for the Mufulira Lufubu Schists.

The Nchanga Granite DO17 is a feldspar porphyric monzogranite and contains accessory, oscillatory zoned allanite, titanite, garnet and ilmenite (Fig. 3D). This granite is slightly peraluminous (Fig. 2B) and is characterized by high Na, K, Rb, Zr, Nb, Y and REE contents, low Ca, Mg content and extremely high HREE concentrations at ~ 10 times the UCC value (Fig. 5B). Nchanga Granite DO17 combines a suprachondritic $^{147}Sm/^{143}Nd$ ratio of 0.205 with a negative present-day εNd of -11 and therefore does not intersect with the depleted mantle evolution curve (Fig. 7).

4.2 Bangweulu and Irumide

4.2.1 Bangweulu and Irumide: magmatic units

The Bangweulu and Irumide magmatic rocks are generally monzogranitic, subalkalic and most are peraluminous (Fig. 2C, D), except monzogranite BGA and meta-andesite BG10 which are slightly metaluminous. All these granitoids show negative Nb, Ta, Zr, Hf, Ti and P anomalies accompanied by positive anomalies of large ion lithophile elements (LILE, e.g., K, Rb and Cs), U, Th and Pb in UCC-normalized spidergrams (Fig. 4B). Their Nb and Y content is relatively homogenous and most rocks plot near the junction between the within plate and syncollisional or arc fields in the Nb-Y diagram (Fig 6B). The Sr and Ba content varies between low values for IR06, IR13 and BG18, and intermediate values for monzogranite BGA and the Mansa Granites (BG01, BG02).

The Kapiri Mposhi Complex IR14 (KMpG) in the SW Irumide Belt is a fine-grained biotite monzogranite (Fig. 9F). It is silica- and sodium- rich (71.5 and 4.07 wt. %), intermediate in alumina and $Fe_2O_{3(T)}$ (15.0 and 2.49 wt. %), K-poor (2.46 wt. % K_2O) and has magnesium number of 37. Figure 5D shows that its HREE content is much lower than the UCC with an elevated La/Lu_{UCC} ratio close to 4. This granite has a present-day Nd isotope composition of -35 εNd and gives a T_{DM} model age of 2.93 Ga (Fig. 7). The monzogranitic IR13, 80 km southeast of the Kapiri Mposhi Complex, also

has a low present-day εNd of -24 and also gives a model age of 2.93 Ga. The latter is also close to the feldspar porphyric Mkushi complex IR11, which contains chalcopyrite mineralizations around quartz grains (Fig. 9E).

The central Irumide Belt monzogranite IR06 shows a foliation defined by coarse-grained muscovites (Fig. 9A) and has a low present-day εNd value of -30 with a T_{DM} age of 3.01 Ga. Another monzogranite from this area, IR07, shows rounded cm-sized biotite-dominated xenocrysts with micaceous reaction rims around opaques (Fig. 9B). The NE Irumide Belt meta-andesite IR04 consists of intensely altered amphibole phenocrysts in a chlorite-rich matrix, while amphibolite IR05 consists mostly of actinolite (Fig. 10C, D). Both NE Irumide Belt metabasites show volcanic arc basalt affinities according to Meshede (1986), yet the higher Ti content in amphibolite IR05 suggests within plate affinities (Fig. 8, Pearce and Cann, 1973, Shervais, 1982). They have present-day εNd values of -16 and -12, with T_{DM} ages of 3.08 and 2.50 Ga, respectively.

Deformed, broken quartz, epidote and titanite in the Mansa Granites BG01 and BG02 indicate intense deformation (Fig. 10A), unlike the granodiorite BG12 in the south central part of the Bangweulu Block (Fig 10B). The Mansa region granites are enriched in REEY compared to the UCC with flat patterns and minor negative Eu anomalies. The associated felsic extrusives (e.g., metarhyolite BG07; Fig 10C) contain sericitized feldspar phenocrysts in a glassy matrix, while the phenocrysts in more mafic units are replaced by epidote and actinolite, contained in a chlorite-rich matrix (e.g., meta-andesite BG10; Fig 10D). The trace element compositions in the Mansa extrusive rocks (BG03, BG07, BG08, BG10) are broadly similar, although the granites have lower Ba, Zr and higher HREE contents compared to the coeval extrusives (Fig. 4E, 5C). The 1870 Ma Mansa granites and extrusives give age-corrected εNd values between -4 and -1 (Fig. 7; De Waele et al., 2006b). The alkali feldspar metarhyolite BG09 gives a higher age-corrected +3 εNd value that reflects the lower Sm/Nd ratio in this metarhyolite.

The South-Central Bangweulu granite BG12 and the migmatitic BG13 are moderately LREE enriched and show pronounced negative Eu-anomalies. They have present-day εNds of -23, with model ages of 3.14 and 2.88 Ga respectively (Fig. 7). The East-Central Bangweulu granitoid BG18 has a present-day εNd value of -16 and an elevated $^{147}Sm/^{144}Nd$ ratio (0.161) that results in an imprecise T_{DM} of 3.62 Ga.

4.2.2 Bangweulu and Irumide: metasedimentary rocks

The quartzites contain highly variable trace element contents, generally with negative Sr, P, Ti and Eu and positive U, Th and Pb anomalies in Post Archean Average Shale (PAAS)-normalized spidergrams (Fig. 4F, G). Their REE content varies in the most pure quartzites varies between 7 and 50 ppm ∑REE, while their Zr content varies between 20.5 and 72 ppm. The feldspar-rich Muva quartzite BGQ contains more REE and Zr (114 and 195 ppm respectively) and shows a relatively flat REEY pattern with a slight LREE enrichment compared to the UCC. The Nsama Fm quartzites BG04 and BG11 have relatively flat, upward concave patterns, while the Kabweluma Fm quartzite BG05 has a quasi-complementary upward convex pattern versus the UCC composition. The Nsama Fm quartzite BG11 and especially the Kabweluma Fm quartzite BG05 show positive Y anomalies, accompanied by negative Eu-anomalies, while the Muva quartzite BGQ displays a pronounced positive Y-anomaly. The Zr/Sc, Th/Sc and Th/La ratios mostly range between 20-90, 1.6-3.8 and 0.17-4.4 respectively. At the inferred ~ 1800 Ma depositional age of the Muva Supergroup (De Waele and Fitzsimons, 2007), the εNd values in the Bangweulu and Irumide metasediments have a wide range between -10 and 0, except for the Nsama Fm siltstone BG14 which has +2 εNd value at this time.

5. Discussion

5.1 Domes region

5.1.1 Western Domes region: evidence for sedimentary cycles and cryptic Archean sources

Lithologically, the Mwombezhi gneisses and migmatites are similar to the Kabompo Dome gneisses which were dated at 1940 ±3 Ma and 1884 ±10 Ma (John, 2001; Key et al., 2001; Liyungu and Njamu, 2000), and similar age ranges are observed in other Domes inliers (e.g., Ngoyi et al., 1991; Rainaud et al., 2002). A recent study by Eglinger (2013) indicated that the Mwombezhi and Solwezi basement contains both ortho- and paragneisses. Paragneisses were identified by multiple age modes of detrital zircons, which constrain a maximum age of deposition at <1515-1475 Ma.

Although the Lumwana gneisses are petrochemically reminiscent of granites, their REEY- and HFSE-contents are uncharacteristically low. Therefore, they are more easily reconciled with meta-arenites (e.g., Spalleti et al., 2012). The high Mg-numbers and low Y/Nb ratios between 0.6 and 1.2 suggest a major proportion of mafic sources for these paragneisses. Such paragneisses are also recognized at Solwezi (Eglinger, 2013) and demonstrate the presence of a regional post-Muva, pre-Katangan sedimentary cycle.

Fine-grained sediments also typically have low Y/Nb ratios (e.g., ~1.4 for PAAS; Pourmand et al., 2012; Taylor and McLennan, 1985), but generally contain elevated REE and HFSE concentrations. The shaley intervals between the gneisses are Cu-(Co) mineralized, and this has been related to metasomatism along shear zones (Bernau et al., 2013). The gneissic units bordering these schistose layers are characterized by elongated sub-cm sized feldspar clasts aligned along the foliation and lack the equidimensional pegmatoid textures in gneisses further away from the schistose parts. On drill core scale, it is unclear whether there is a tectonic contact or a preferential accommodation of strain near the schistose units (e.g., Bernau et al., 2013). Therefore, it cannot be excluded that the mineralized schistose parts are in fact Katanga sequence units that were tectonically interlayered with the Mwombezhi basement during the Lufilian Orogeny (Cosi et al., 1992).

Most felsic Chimiwungo prospect gneisses and one Lumwana gneiss (DO04) have a major- and trace element composition and mineralogy consistent with an orthogneissic origin. Their T_{DM} model ages range between c. 2.2 and 3.1 Ga and thus predate the Paleoproterozoic igneous ages in the Domes region considerably. This suggests that their igneous protoliths have considerable crustal residence times. This is also consistent with igneous model ages from Eglinger (2013), who calculates 2.4-2.9 Ga zircon εHf model ages with a minor component between 3.0 and 3.6 Ga.

The geochemical characteristics of the Mwombezhi amphibolite are similar to those of the Katangan tholeite and alkali basalt suite related to rifting in the Domes region at 765-735 Ma (Fig. 8; Key et al., 2001; Tembo et al., 1999). The Ti-V characteristics preclude an arc-related igneous origin, as these typically have much lower Ti/V ratios and contents (Fig. 8). Similar units are also reported in the Mwombezhi and Solwezi Domes by Eglinger (2013). Their position within the Mwombezhi paragneisses implies an age younger than c. 1500 Ma, as indicated by detrital zircons within these

gneisses (Eglinger, 2013). These amphibolites potentially belong to the Neoproterozoic tholeite suite, but this needs to be confirmed with radiometric dating.

The younger model age of 1.93 Ga in the Lumwana East Granite is attributed to relative LREE enrichment decreasing Sm/Nd, during intense post-igneous alteration, likely in oxidizing conditions as indicated by the pronounced negative Ce-anomaly. The Ca, Sr and Ba-poor composition of the Lumwana East Granite is probably related to the sericitization of the feldspars, whereas the high LREE content in this granite is contained in the LREE-selective allanite. The high Th-low U characteristics of this granite likely result from U mobilization towards the uranium deposits rimming the Mwombezhi Dome, i.e. this granitoid and similar ones are likely sources for the uranium in these deposits (e.g., Eglinger et al., 2013).

5.1.2 Eastern Domes region: arc terranes and intracratonic magmatism ?

Model ages for the Kafue basement region are similar to those in the Mwombezhi Dome, indicating that both inliers have similar crustal residence times, with an important Archean component. The petrographic data for the Mufulira Lufubu Schist samples DO19 and DO20 indicates that they are likely not of extrusive origin since they lack typical extrusive textures or contain tourmaline. While it cannot be excluded that the Nkana Lufubu Schist NSD49 has a volcanic protolith, a sedimentary origin seems more likely, given its petrological characteristics. From a Copperbelt metal source perspective, this unit is interesting, as it underlies the Neoproterozoic Nkana Cu-Co deposit. Its high-Co, low-Cu composition is likely not primary and is attributed to intense metasomatic alteration related to the hydrothermal ore-forming processes. Differential mobility of Co and Cu during reworking commonly results in Cu-Co fractionation (e.g., De Putter et al., 2010, Torremans et al., 2013).

The Mufulira Grey Granite is estimated at ~1950 Ma (see section 4.1.2) and is spatially associated with the Mufulira Lufubu schists, which have been dated at 1968 ±9 Ma (Lobo-Guerrero Sanz, 2005; Rainaud et al., 2005). Based on these spatial associations, Rainaud et al. (2005) suggested that the metavolcanic Lufubu Schists and their plutonic contemporaries represent one or several magmatic arc terranes. The age-corrected εNd values in the eastern Domes granitoids are around -4 to -2 and

preclude an island arc setting, since εNd values around 5 are expected from island arcs originating from the depleted mantle (DePaolo, 1981; Fig. 7).

The Tshinsenda and Mufulira granites are petrochemically reminiscent of arc-related granites. They are relatively Si-poor and relatively rich in ferromagnesic elements. Furthermore, the epidote-chlorite-magnetite clusters within these granitoids could respresent an alteration of hornblende. This mineral typically characterizes arc-related granites and relict hornblende was reported in Lufubu metavolcanics (Babarin, 1999; Rainaud et al., 2005). Therefore, it seems plausible that these Paleoproterozoic granites are placed in a continental arc setting, where they rework older crustal material.

The Neoproterozoic Nchanga granite was dated at 880 Ma and occurs as a NW-SE oriented 10 by 15 km ellipsoid pluton in the northwestern part of the Kafue Basement Complex (Armstrong et al., 2005; Katongo et al., 2004). The geochemical characteristics of the Nchanga Granite with high alkali, REE, Nb and low Ca, Mg are consistent with an anorogenic origin (e.g., Eby, 1992; Trumbull et al., 2004). This is also indicated by elevated Ga/Al ratios (Katongo et al., 2004; Lobo-Guerrero Sanz, 2005). Most parts of the pluton display low Nb/Y ratios characteristic of a dominant crustal protolith, while some parts display elevated, MORB-like Nb/Y ratios (e.g., Katongo et al., 2004; Lobo-Guerrero Sanz, 2005). The HREE-enrichment and suprachondritic $^{157}Sm/^{144}Nd$ ratio in this granite is likely related to intense alteration during albitization in sample DO17.

A high mantle contribution is not atypical for anorogenic granite suites which are often characterized by variable amounts of mixing between a crustal and a mantle source (e.g., Trumbull et al., 2004). However, Katongo et al. (2004) infer that this granite intruded during early stages of rift development where mantle involvement is usually minimal. In the context of our Nd isotope data, this would require that the present-day suprachondritic Sm/Nd ratio was generated close to its igneous age at 880 Ma (Armstrong et al., 2005). The present-day εNd of -11 corresponds closely to the average crustal Nd composition of the domes samples at that time, and this would have evolved at a CHUR-like rate (Fig. 7). Therefore, the elevated εNd would only imply a significant contribution from mantle material if the high Sm/Nd ratio was generated much later.

5.2 Bangweulu-Irumide region

5.2.1 Evidence for reworking of Archean sources

The geochemical characteristics of the Kapiri Mposhi Complex correspond closely to the tonalite trondjhemite granodorites (TTG) of the G_0 group defined by De Waele et al. (2006b) who dated the Kapiri Mposhi complex at 2726 ±36 Ma (De Waele, 2005). De Waele et al. (2006b) attribute the low HREE content to melting in the presence of garnet, for instance by melting of the eclogitized parts of a subducting oceanic slab. They point out that this is incompatible with the negative Nb anomaly (Fig 4D), which suggests mantle melting in the presence of aqueous fluids. However, experimental data suggests that melting in the stability field of garnet and hornblende can generate HREE and Nb depleted melt compositions, as the latter incorporates Nb (e.g., Martin et al., 2005). Since modern analogues for TTGs are mainly formed by slab melting with subordinate contamination from mantle peridotite (Martin et al., 2005), we argue in favor of such an origin for the Kapiri Mposhi Complex. The 2.93 Ga T_{DM} exceeds its crystallization age and indicates contribution from more enriched mantle domains or involvement of Mesoarchean crust.

Earlier studies noted that post-Archean granitoids are geochemically similar in the Irumide and Bangweulu regions (De Waele et al., 2006b; Tembo et al., 2002), and this is confirmed by this study (Fig. 4D). Their trace element patterns show low HFSE contents typical for magmatics with a crustal origin (e.g., De Waele et al., 2006b; Hofmann, 1997). All granites show the typical negative Ti and P anomalies related to titanite or ilmenite and apatite fractionation, while plagioclase fractionation accounts for their negative Eu-anomalies and low Sr and Ba content, as noted by De Waele et al. (2006b). The main difference between our results and those of De Waele et al. (2006b) is that around 1870 Ma our Mansa magmatics have more enriched Nd compositions (-4 to -2 versus -7 to -4) and younger model ages (2.3-2.5 Ga versus 2.5-2.9 Ga). This suggests a sub-suite with more input of juvenile material in this region, with similar model ages as those in contemporaneous Irumide extrusives (De Waele et al., 2006b).

The Mesoproterozoic G_4 group is restricted to the Irumide Belt, and is geochemically and isotopically similar to the G_1 granitoids. Because the G_1 and G_4 groups melt sources with similar compositions, they are hard to distinguish (De Waele et al., 2006b). Therefore, it is not possible to identify if Irumide

granitoids IR06 and IR13 belong to the G_1 or G_4 group, except by radiometric dating. In any case, geochemical compositions and T_{DM} model ages for the Irumide granitoids are similar to those in the Bangweulu Block, except in the Mansa magmatics (Fig. 7). This corroborates both the Archean inheritance and the relationship between the Bangweulu and the Irumide Belt proposed by De Waele et al. (2006b).

5.2.2 Locally sourced metasedimentary units?

The Bangweulu and the Irumide were essentially one tectonic unit during deposition of the Paleoproterozoic sedimentary successions, which correlate across these basement blocks (e.g., De Waele et al., 2001). The depositional setting and correlations between the sedimentary sequences is extensively treated in e.g., Andersen and Unrug (1984), De Waele and Mapani (2002) and De Waele and Fitzsimons (2007). This study provides an overview of the chemical composition of these sediments. Most elemental anomalies mimic the ones in the Bangweulu and Irumide granites, with the exception of Nb and Ta, whose anomalies are far less pronounced. Apart from the Nsama Fm siltstone BG14, all metasedimentary units show high Zr, Hf and high Th/Sc, Zr/Sc and low La/Th ratios indicative for crustal or passive margin sedimentary sources (e.g., Spaletti et al., 2012).

The Nsama Fm siltstone has a high εNd(T) value of 2. In combination with its elevated concentrations of ferromagnesic elements, this suggests a major contribution from a mafic source. The age-corrected εNd values and the Nd model ages of the other sediments suggest sedimentary sources with crustal residence times that are significantly higher than 1800 Ma, the approximate depositional age for these sediments (De Waele et al., 2006b). This data suggests that these metasediments are locally sourced from the Bangweulu and Irumide magmatics.

5.3 Implications for interregional cratonic relationships

Several authors proposed a relationship between the Domes region and the Bangweulu Block or the Irumide Belt based on the contemporaneity of the magmatic phases (e.g., De Waele et al., 2006b; Eglinger, 2013; Rainaud et al., 2005). For the ~1870 Ma Ubendian phase, this is further corroborated

by association of intrusives and extrusives that indicates shallow intrusion in these regions (e.g., De Waele et al., 2006b; Rainaud et al., 2005). Additionally, T_{DM} ages indicate reworking of Archean crustal components in all terranes. The model ages for the eastern Domes magmatic rocks indicate similar average crustal residence times as those of the SW Bangweulu magmatic rocks (Fig. 7; De Waele et al. 2006b). Geochemically, the eastern Domes magmatics are more similar to the intermediate SW Bangweulu extrusives than to their silica-rich intrusive counterparts and lack the pronounced Pb anomaly (Fig. 4B,E), indicating that the crustal contribution is less prominent here. The oldest model age components in the E Domes and SW Bangweulu appear less prominent than in other regions, for instance the SW Irumide. This is consistent with juvenile input in a continental arc setting. The cluster of c. 3 Ga model ages in the SW Irumide likely relates to an older nucleus centered around the Archean Kapiri Mposhi Complex (e.g., De Waele et al., 2006b).

Although estimates for average crustal residence times are highly variable in each region, they are broadly comparable between all regions, suggesting a relationship between the Domes and the Bangweulu, including its metacratonized margin, the Irumide Belt. Moreover, T_{DM} ages above 2.5 and 2.3 Ga in all terranes indicate that juvenile input is relatively limited after the Ubendian phase. This suggests an intracratonic setting for these terranes from c. 1870 Ma onwards. However, renewed juvenile input in the Domes region is evidenced by rift-related tholeites at 750-735 Ma (e.g., Key et al., 2001; Tembo et al., 1999). Radiometric dating of the Mwombezhi and Solwezi amphibolites is required to determine whether these belong to this suite or represent an earlier phase of juvenile input.

5.4 Implications for metal provenance studies

The Neoproterozoic Katanga sediments in the Copperbelt region host abundant economic Cu-Co deposits. Mass balance calculations suggest that the Neoproterozoic Katanga sediments that host these deposits are unable to provide sufficient metals to act as the principal source (e.g., Cailteux et al., 2005; Hitzman et al., 2000). An extensive review by Sweeney et al. (1991) shows that some basement units may contain significant amounts of Cu, besides the sulfide-hosted copper in basement deposits such as the Lumwana and Mkushi deposits. This dataset and similar datasets (e.g., De Waele et al., 2006b; Duchesne et al., 2004; Johnson et al., 2007b) can be used in combination with isotope analyses

of gangue carbonates associated with the Copperbelt ore deposits to test the basement's source potential (e.g., Van Wilderode et al., 2014). Because the Rb-Sr system is readily perturbed, it is preferably used as a potential extra discriminating factor in combination with the Nd isotope signature. For instance, the Mwombezhi paragneisses and Lufubu Schists can be distinguished from the felsic Bangweulu and Irumide units, as they generally have higher age-corrected Nd isotope values at the Neoproterozoic mineralization times. The results from Van Wilderode et al. (2014) show that the gangue minerals correspond more closely to the Mwombezhi paragneisses or Lufubu Schist signatures, suggesting local Cu sourcing from the basement units directly below the Copperbelt.

6. Conclusions

Our integrated whole rock petrochemical and Sm-Nd isotopic approach offers more evidence for reworking of (cryptic) Archean crustal material in the Domes inliers at depth below the Neoproterozoic Central African Copperbelt and in the Bangweulu-Irumide region. The data for the eastern Domes granitoids and similar magmatic units in the SW Bangweulu Block corroborates earlier studies that suggest a mid-Paleoproterozoic arc terrane (De Waele et al., 2006b; Rainaud et al., 2005). Moreover, the available petrochemical and isotopic data is consistent with a mid-Paleoproterozoic continental arc, but precludes an island arc, since the isotope ratios indicate incorporation of older crustal material. Finally, Archean and early-Paleoproterozoic model ages in all terranes indicate limited juvenile input from the mid-Paleoproterozoic onwards, implying mostly intracratonic positions during subsequent magmatic phases. The broadly similar crustal residence times suggest a relationship between the Domes region inliers and the Bangweulu-Irumide terrane.

ACKNOWLEDGEMENTS

We are grateful to Mike Richards (Equinox) and Barrick Gold for providing the Mwombezhi samples and Dr. Stijn Dewaele from the Royal Museum for Central Africa in Tervuren for providing additional E Domes and Bangweulu samples. Constructive comments from two 'Journal of African Earth Science' reviewers significantly improved key issues. We also like to thank Dr. Simon Johnson, Dr. Bert De Waele, Prof. Jan Hertogen, Prof. Marlina Elburg, Dr. Osbert Sikazwe, Drs. Niels Hulsbosch

and Mr. Willy Nundwe for their assistance, the stimulating discussions and constructive criticism that greatly improved this manuscript. We thank Herman Nijs for preparing high-quality thin sections and Dr. Elvira Vassilieva for her analytical expertise. David Debruyne is a research assistant of the Fund for Scientific Research – Flanders (FWO-Flanders). Jorik Van Wilderode is a research assistant funded by the Agency for Innovation by Science and Technology (IWT), research grant ZKC2784-00-W01. Additional financial support from the Lu-Hf and Sm-Nd project grant G.A078.11N from FWO Flanders is gratefully acknowledged.

7. References

Abdelsalam, M., Liégeois, J.P., Stern, R.J., 2002. The Saharan metacraton, Journal of African Earth Sciences 34, 119-136.

Andersen, L.S., Unrug, R., 1984. Geodynamic evolution of the Bangweulu Block, northern Zambia. Precambrian Research 25, 187-212.

Armstrong, R.A., Master, S., Robb, L.J., 2005. Geochronology of the Nchanga Granite, and constraints on the maximum age of the Katanga Supergroup, Zambian Copperbelt. Journal of African Earth Sciences 42, 32-40.

Barbarin, B., 1999. A review of the relationships between granitoid types, their origins and their geodynamic environments. Lithos 46, 605-626.

Bernau, R., 2007. The geology and geochemistry of the Lumwana basement hosted copper-cobalt (uranium) deposits, NW Zambia. Unpublished PhD thesis, University of Southampton, UK.

Bernau, R., Roberts, S., Richards, M., Nisbet, B., Boyce, A., Nowecki, J., 2013. The geology and geochemistry of the Lumwana Cu (± Co ± U) deposits, NW Zambia. Mineralium Deposita 48, 137-153.

Bevington P.R., Robinson, D.K., 1992. Data reduction and error analysis for the physical sciences, 3rd ed. McGraw-Hill, New York.

Black, R., Liégeois, J.P., 1993. Cratons, mobile belts, alkaline rocks and continental lithospheric mantle: the Pan-African testimony, Journal of the Geological Society of London 150, 89–98.

Brandt, R., Burton, C.C.J., Maree, S.C., Woakes, M.E., 1961. Mufulira, in: The Geology of the Northern Rhodesian Copperbelt. MacDonald, London, pp. 411-461.

Brewer, M.S., Haslam, H.W., Darbyshire, P.F.P., Davis, A.E., 1979. Rb-Sr Age Determinations in the Bangweulu Block, Luapula Province, Zambia, vol. 79/5, Institute of Geological Sciences, London.

Cahen, L., Delhal, J., Deutsch, S., Grögler, N., Pasteels, P., 1970. The age of the Roan Antelope and Mufulira granites (Copperbelt of Zambia), Annales du Musée Royal de l'Afrique Centrale, Sciences Géologiques 65, 15-42.

Cailteux, J., Kampunzu, A., Lerouge, C., Kaputo, A., Milesi, J., 2005. Genesis of sediment-hosted stratiform copper–cobalt deposits, central African Copperbelt. Journal of African Earth Sciences 42, 134-158

Cosi M., Debonis A., Gosso G., Hunziker J., Martinotti G., Moratto S., Robert J.P., Ruhlman F., 1992. Late proterozoic thrust tectonics,high-pressure metamorphism and uranium mineralization in the domes area, Lufilian Arc, northwestern Zambia. Precambrian Research 58, 215-240.

Clark, G.S., Černý, P., 1987. Radiogenic ^{87}Sr, its mobility, and the interpretation of Rb-Sr fractionation trends in rare-element granitic pegmatites. Geochimica et Cosmochimica Acta 51, 1011-1018.

Daly, M.C., 1986. The tectonic and thermal evolution of the Irumide belt, Zambia. (Unpublished). University of Leeds.

De Muynck, D., Huelga-Suarez, G., Heghe, L.V., Degryse, P., Vanhaecke, F., 2009. Systematic evaluation of a strontium-specific extraction chromatographic resin for obtaining a purified Sr fraction with quantitative recovery from complex and Ca-rich matrices. Journal of Analytical Atomic Spectrometry 24, 1498-1510.

De Putter, T., Mees, F., Decrée, S., Dewaele, S., 2010. Malachite, an indicator of major Pliocene Cu remobilization in a karstic environment (Katanga, Democratic Republic of Congo). Ore Geology Reviews 38, 90-100.

De Waele, B., Fitzsimons, I.C.W., 2007. The nature and timing of Palaeoproterozoic sedimentation at the southeastern margin of the Congo Craton; zircon U–Pb geochronology of plutonic, volcanic and clastic units in northern Zambia. Precambrian Research 159, 95-116.

De Waele, B., Mapani, B., 2002. Geology and correlation of the central Irumide belt. Journal of African Earth Sciences 35, 385-397.

De Waele, B., Tembo, F., Wingate, M.T.D., 2001. A review of the geochronology of the Irumide Belt, Zambia. Presented at the Fourth International Archean Symposium, Perth, Australia, pp. 303-305.

De Waele, B., Johnson, S.P., Nkemba, S., Tembo, F., 2005. High-temperature, low-pressure tectono-thermal evolution of the Irumide Belt, central Southern Africa: lithosphere delamination during arc-accretion. Frontier Research on Earth Evolution 2, 9.

De Waele, B., Liégeois, J.-P., Nemchin, A.A., Tembo, F., 2006a. Isotopic and geochemical evidence of proterozoic episodic crustal reworking within the irumide belt of south-central Africa, the southern metacratonic boundary of an Archaean Bangweulu Craton. Precambrian Research 148, 225–256.

De Waele, B., Kampunzu, A.B., Mapani, B.S.E., Tembo, F., 2006b. The Mesoproterozoic Irumide belt of Zambia. Journal of African Earth Sciences 46, 36-70.

De Waele, B., Johnson, S.P., Pisarevsky, S.A., 2008. Palaeoproterozoic to Neoproterozoic growth and evolution of the eastern Congo Craton: Its role in the Rodinia puzzle. Precambrian Research 160, 127-141.

De Waele, B., Fitzsimons, I.C.W., Wingate, M.T.D., Tembo, F., Mapani, B., Belousova, E.A., 2009. The geochronological framework of the Irumide Belt: A prolonged crustal history along the margin of the Bangweulu Craton. American Journal of Science 309, 132-187.

DePaolo, D.J., 1981. Neodymium isotopes in the Colorado Front Range and crust–mantle evolution in the Proterozoic. Nature 291, 193-196.

Duchesne, J.-C., Liégeois, J.-P., Deblond, A., Tack, L., 2004. Petrogenesis of the Kabanga-Musongati layered mafic-ultramafic intrusions in Burundi (Kibaran Belt): geochemical, Sr-Nd isotopic constraints and Cr-Ni behaviour. Journal of African Earth Sciences, 39, 133-145.

Eby, G.N., 1992. Chemical subdivision of the A-type granitoids: Petrogenetic and tectonic implications. Geology 20, 641-644.

Eglinger, A., 2013. Uranium cycle and tectono-metamorphic evolution of the Lufilian belt (Zambia). PhD thesis, Unversité de Lorraine, Nancy.

Eglinger, A., André-Mayer, A.-S., Vanderhaeghe, O., Mercadier, J., Cuney, M., Decrée, S., Feybesse, J.-L., Milesi, J.-P., 2013. Geochemical signatures of uranium oxides in the Lufilian belt: From unconformity-related to syn-metamorphic uranium deposits during the Pan-African orogenic cycle. Ore Geology Reviews 54, 197-213.

Farmer, G.L., DePaolo, D.J., 1983. Origin of Mesozoic and Tertiary Granite in the Western U. S. and Implications for Pre-Mesozoic Crustal Structure. 1. Nd and Sr Isotopic Studies in the Geocline of the Northern Great Basin. Journal of Geophysical Research 88, 3379-3401.

Fitches, W.R., 1971. Sedimentation and tectonics at the northern end of the Irumide orogenic belt, N. Malawi and Zambia. Geologische Rundschau 59, 444-458.

Ganio, M., Latruwe, K., Brems, D., Muchez, P., Vanhaecke, F., Degryse, P., 2012. The Sr-Nd isolation procedure for subsequent isotopic analysis using multi-collector ICP-mass spectrometry in the context of provenance studies on archaeological glass. Journal of Analytical Atomic Spectrometry 27, 1335-1341.

Hitzman, M.W., 2000. Source basins for sediment-hosted stratiform Cu deposits: implications for the structure of the Zambian Copperbelt. Journal of African Earth Sciences 30, 855-863.

Hofmann, A.W., 1997. Mantle geochemistry: the message from oceanic volcanism. Nature 385, 219-229.

John, T., 2001. Subduction and continental collision in the Lufilian Arc–Zambezi belt orogen: a petrological, geochemical, and geochronological study of eclogites and whiteschists (Zambia). PhD thesis, University of Kiel, Kiel.

Johnson, SP and Oliver, GJH, 2004, Tectonothermal history of the Kaourera Arc, northern Zimbabwe, with implications for the tectonic evolution of the Irumide and Zambezi Belts of south central Africa, Precambrian Research, 130, 71-97.

Johnson, SP, Rivers, T and De Waele, B, 2005, A review of the Mesoproterozoic to early Palaeozoic magmatic and tectonothermal history of south-central Africa: implications for Rodinia and Gondwana: Journal of the Geological Society of London 162, p. 433-450.

Johnson, SP, De Waele, B and Liyungu, KA, 2006, U-Pb sensitive high-resolution ion microprobe (SHRIMP) zircon geochronology of granitoid rocks in eastern Zambia: Terrane subdivision of the Mesoproterozoic Southern Irumide Belt: Tectonics, 25, p. TC6004, doi:10.1029/2006TC001977.

Johnson, SP, De Waele, B, Evans, D, Tembo, F, Banda, W, Milton, JA and Tani, K, 2007a, Geochronology of the Zambezi Supracrustal sequence, southern Zambia: A record of Neoproterozoic divergent processes along the southern margin of the Congo Craton, Journal of Geology, 115, 355-374.

Johnson, SP, De Waele, B, Tani, K, Tembo, F, Chang, Q, Iizuka, T and Dunkley, D, 2007b, Geochemistry, geochronology and isotopic evolution of the Chewore-Rufunsa Terrane, Southern Irumide Belt: A Mesoproterozoic continental-margin-arc, Journal of Petrology 48, 1411-1441.

Kabengele, M., Lubala, R.T., Cabanis, B., 1991. Caractérisation pétrologiques et géochimique du magmatisme ubendien du secteur de Pepa-Lubumba, sur le plateau des Marungu (Nord-Est du Shaba, Zaire). Signification géodynamique dans l'évolution de la chaine ubendienne. Journal of African Earth Sciences 13, 243-265.

Katongo, C., Koller, F., Kloetzli, U., Koeberl, C., Tembo, F., De Waele, B., 2004. Petrography, geochemistry, and geochronology of granitoid rocks in the Neoproterozoic-Paleozoic Lufilian-Zambezi belt, Zambia: Implications for tectonic setting and regional correlation. Journal of African Earth Sciences 40, 219-244.

Key, R.M., Liyungu, A.K., Njamu, F.M., Somwe, V., Banda, J., Mosley, P.N., Armstrong, R.A., 2001. The western arm of the Lufilian Arc in NW Zambia and its potential for copper mineralization. Journal of African Earth Sciences 33, 503-528.

Liégeois, J.-P., Abdelsalam, M.G., Ennih, N., Ouabadi, A., 2013. Metacraton: Nature, genesis and behavior, Gondwana Research 23, 220-237.

Liyungu, A.K., Njamu, F.J., 2000. The geology of the Lumwana West area. Explanation of Degree Sheet 1125, SW Quarter. Geological Survey Department, Zambia, Report No. 111, 44pp.

Lobo-Guerrero Sanz, A., 2005. Pre-and post-Katangan granitoids of the greater Lufilian arc - geology, geochemistry, geochronology and metallogenic significance. PhD thesis, Wits University, Johannesburg.

Mareels, J., 2004. ICP – MS analysis, geochemistry and petrogenesis of granites from the Variscan Northern Vosges (France) PhD thesis, KU Leuven, Leuven.

Martin, H., Smithies, R.H., Rapp, R., Moyen, J.F., Champion, D., 2005. An overview of adakite, tonalite-trondhjemite-granodiorite (TTG), and sanukitoid: relationships and some implications for crustal evolution. Lithos 79, 1-24.

McDonough, W.F., Sun, S., 1995. The composition of the Earth. Chemical Geology 120, 223-253.

McLennan, S.M., Xiao, G., 1998. The composition of the continental crust revisited: insights from sedimentary rocks, abstract, Mineralogical Magazine 62A, 982-984.

Mendelsohn, F., 1961. The Geology of the Northern Rhodesia Copper belt. MacDonald, London.

Meschede, M., 1986. A method of discriminating between different types of mid-ocean ridge basalts and continental tholeiites with the Nb-Zr-Y diagram. Chemical Geology 56, 207-218.

Nelson, B.K., DePaolo, D.J., 1985. Rapid production of continental crust 1.7-1.9 b.y. ago: Nd and Sr isotopic evidence from the basement of the North American midcontinent. Bulletin Geological Society of America 96, 746-754.

Ngoyi, K., Liégeois, J.-P., Demaiffe, D., Dumont, P., 1991. Age tardi-ubendien (Protérozoïque inférieur) des dômes granitiques de l'arc cuprifère zaïro-zambien. Comptes Rendus de l'Académie des Sciences de Paris 313, 83-89.

Pearce, J.A., Cann, J.R., 1973. Tectonic setting of basic volcanic rocks determined using trace element analyses. Earth and Planetary Science Letters 290-300.

Pearce, J.A., Harris, N.B.W., Tindle, A.G., 1984. Trace Element Discrimination Diagrams for the Tectonic Interpretation of Granitic Rocks. Journal of Petrology 25, 956–983.

Pin, C., Briot, D., Bassin, C., Poitrasson, F., 1994. Concomitant separation of strontium and samarium-neodymium for isotopic analysis in silicate samples, based on specific extraction chromatography. Analytica Chimica Acta 298, 209-217.

Porada, H., Berhorst, V., 2000. Towards a new understanding of the Neoproterozoic-early palæozoic Lufilian and northern Zambezi belts in Zambia and the Democratic Republic of Congo. Journal of African Earth Sciences 30, 727–771.

Pourmand, A., Dauphas, N., Ireland, T.J., 2012. A novel extraction chromatography and MC-ICP-MS technique for rapid analysis of REE, Sc and Y: Revising CI-chondrite and Post-Archean Australian Shale (PAAS) abundances. Chemical Geology 291, 38–54.

Rainaud, C., Armstrong, R.A., Robb, L.J., Mumba, P.A.C.C., 2002. Contributions to the geology and mineralisation of the central African Copperbelt: I. Nature and geochronology of the pre-Katangan basement. In: Namibia, G.S.O. (Ed.), Geological Survey of Namibia, 11th IAGOD Quadrennial Symposium and Geocongress, Windhoek, Namibia, p. 5.

Rainaud, C., Master, S., Armstrong, R.A., Robb, L.J., 2003. A cryptic Mesoarchaean terrane in the basement to the Central African Copperbelt. Journal of the Geological Society 160, 11-14.

Rainaud, C., Master, S., Armstrong, R., Robb, L., 2005. Geochronology and nature of the Palaeoproterozoic basement in the Central African Copperbelt (Zambia and the Democratic Republic of Congo), with regional implications. Journal of African Earth Sciences 42, 1-31.

Rudnick, R.L., Gao, S., 2003. Composition of the Continental Crust, in: Treatise on Geochemistry. Elsevier, pp. 1-64.

Schandelmeier, H., 1980. Regionale gliederung des Prakambriums und aspekte der krustentwicklung um Mambwe/nordost-Zambia. PhD thesis, Technical University of Berlin, Berlin.

Schandelmeier, H., 1983. The geochronology of post-Ubendian granitoids and dolerites from the Mambwe area. Northern Province, Zambia. Institute of Geological Sciences 83, 40-46.

Selley, D., Broughton, D., Scott, R.J., Hitzman, M., Bull, S.W., Large, R.R., McGoldrick, P.J., Croaker, M., Pollington, N., 2005. A New Look at the Geology of the Zambian Copperbelt. Economic Geology 100th Anniversary Volume, 965-1000.

Shervais, J.W., 1982. Ti-V plots and the petrogenesis of modern and ophiolitic lavas. Earth and Planetary Science Letters 59, 101-118.

Spalletti, L.A., Limarino, C.O., Piñol, F.C., 2012. Petrology and geochemistry of Carboniferous siliciclastics from the Argentine Frontal Cordillera: A test of methods for interpreting provenance and tectonic setting. Journal of South American Earth Sciences 36, 32-54.

Sweeney, M.A., Binda, P.L., Vaughan, D.J., 1991. Genesis of the ores of the Zambian Copperbelt. Ore Geology Reviews 6, 51-76.

Tanaka, T., Togashi, S., Kamioka, H., Amakawa, H., Kagami, H., Hamamoto, T., Yuhara, M., Orihashi, Y., Yoneda, S., Shimizu, H., Kunimaru, T., Takahashi, K., Yanagi, T., Nakano, T., Fujimaki, H., Shinjo, R., Asahara, Y., Tanimizu, M., Dragusanu, C., 2000. JNdi-1: a neodymium isotopic reference in consistency with LaJolla neodymium. Chemical Geology 168, 279-281.

Taylor, S.R., McLennan, S.M., 1985. The Continental Crust: Its Composition and Evolution. Blackwell Science, Oxford, 312 pp.

Tembo, F., Kampunzu, A.B., Porada, H., 1999. Tholeiitic magmatism associated with continental rifting in the Lufilian Fold Belt of Zambia. Journal of African Earth Sciences 28, 403-425.

Tembo, F., De Waele, B., Nkemba, S., 2002. Syn- to post-orogenic granitoid magmatism in the Irumide Belt of Zambia: geochemical evidence. African Geology Reviews 9, 1-17.

Thirlwall, M.F., 1991. Long-term reproducibility of multicollector Sr and Nd isotope ratio analysis. Chemical Geology: Isotope Geoscience section 94, 85-104.

Torremans, K., Gauquie, J., Boyce, A.J., Barrie, C.D., Dewaele, S., Sikazwe, O., Muchez, P., 2013. Remobilisation features and structural control on ore grade distribution at the Konkola stratiform Cu-Co ore deposit, Zambia. Journal of African Earth Sciences 79, 10-23.

Trumbull, R.B., Harris, C., Frindt, S., Wigand, M., 2004. Oxygen and neodymium isotope evidence for source diversity in Cretaceous anorogenic granites from Namibia and implications for A-type granite genesis. Lithos 73, 21-40.

Van Wilderode, J. El Desouky, H.A., Elburg, M.A., Vanhaecke, F., Muchez Ph., 2014. Metal sources for the Congolese Central African Copperbelt deposits: insights from Sr and Nd isotope ratios. Geologica Belgica 17, 137-147.

Whitney, D.L., Evans, B.W., 2010. Abbreviations for names of rock-forming minerals. American Mineralogist 95, 185-187.

8. Figure captions

Figure 1. Simplified geological map with the sample locations in the Bangweulu Block, the Domes inliers and the Irumide Belt. Depleted mantle Nd model ages (in Ga) are also shown: model ages for altered igneous units are in italic (see 4.2.1, 5.1.1); model ages for metasedimentary units are indicated

between brackets. Modified from Andersen and Unrug (1984), De Waele et al. (2006a, 2006b) and Tembo et al. (1999).

Figure 2. Diagrams showing the major element composition of the studied samples. (A) and (C) plot the normative quartz-alkalifeldspar-plagioclase (QAP) composition of the Domes (DO) and Bangweulu and Irumide (BG and IR) samples respectively. (B) and (D) show the aluminum saturation index (A/CNK) versus the agpaitic index (A/NK) for the DO and BG + IR samples respectively. Abbreviations (A, B): MwG, Mwombezhi gneisses; MwA, Mwombezhi amphibolite; LS, Lufubu Schist, LEG, Lumwana East Granite; TsG, Tshinsenda Granitoids; MGG, Mufulira Grey Granite; NG, Nchanga granite. Includes additional Nchanga granite data from Katongo et al. (2004) and Lobo-Guerrero Sanz (2005) for comparison. Abbreviations (B, E): BG, Bangweulu, IR, Irumide; G, granitoids; sed, metasediments; maf, mafics; MmV, Mansa metavolcanites; KmPG,Kapiri Mposhi Granite Complex. Normative compositions calculated using Igpet (2005).

Figure 3. Representative microphotographs of the studied Domes region samples. (A) Hornblende, plagioclase, biotite and minor titanite in Mwombezhi amphibolite DO01 (PPL). (B) Typical Mwombezhi paragneiss DO04 with opaques and exsolutions in feldspars coexisting with biotite and muscovite (PPL). (C) Epidote, magnetite and chlorite could represent a metamorphically altered hornblende in Tshinsenda monzogranite DO14. Biotite shows rutile exsolutions and pleochroitic halos around zircon or monazite inclusions (XPL). (D) Nchanga granite with cm-sized microcline showing perthitic unmixing and micaceous reaction rims around opaques (XPL). (E) Mufulira Grey Granite with sericitized feldspars, quartz with subgrains, biotite, skeletal titanite and accessory epidote (XPL). (F) Mufulira Lufubu schist with feldspar laths, tourmaline, biotite and chlorite (PPL). PPL, parallel polars; XPL, crossed polars; mineral abbreviations after Whitney and Evans (2010).

Figure 4. Primitive mantle (PM) normalized spidergrams for the analyzed samples. (A) Mwombezhi gneisses, (B) Domes region granitoids, (C) Domes and Irumide mafics, (D) Bangweulu and Irumide granitoids, (E) Mansa region magmatics, (F) Bangweulu metasediments and (G) Irumide

metasediments. Abbreviations as in Figure 2, except LUM, Lumwana; CHI, Chimiwungo. The grey shaded areas correspond to the compositional range of the G_1-group granites from De Waele et al. (2006b). PM composition after McDonough and Sun (1989). Post Archean Average Shale (PAAS) composition compiled from Taylor and McLennan (1985), McLennan and Xiao (1998) and Pourmand et al. (2012).

Figure 5. Upper Continental Crust (UCC) normalized REEY plots. (A) Domes region granitoids, (B) Mwombezhi gneisses, (C) Mansa magmatics and (D) Bangweulu and Irumide granitoids. Abbreviations as in Figure 2. The grey shaded areas correspond to the compositional range of the G_1-group granites from De Waele et al. (2006a, b). UCC composition after Rudnick and Gao (2003).

Figure 6. Nb-Y diagram from Pearce et al. (1984). (A) Domes samples, with indicated sample numbers for the Mwombezhi gneisses and additional Nchanga Granite data from Katongo et al. (2004) and Lobo-Guerrero Sanz (2005). (B) the Irumide and Bangweulu samples. The G_1 group granites from De Waele et al. (2006b) are added for comparison. Abbreviations as in Figure 2.

Figure 7. Nd evolution diagram for the Domes samples (left) and Irumide and Bangweulu samples (right). Depleted mantle from Nelson and DePaolo (1985). Indicated events from Armstrong et al., 2005; De Waele et al., 2006b; De Waele and Fitzsimons, 2007; Eglinger, 2013; Key et al., 2001, Rainaud et al., 2005.

Figure 8. Ti-V diagram from Shervais (1982) for the Domes, Irumide and Bangweulu mafics. The grey fields indicate typical compositions for mafic units in different tectonic settings, including mid-oceanic ridge and back arc basin basalts (MORB and BAB) according to Shervais (1982). Also shown are the compositions of rift-related Neoproterozoic Domes region tholeites from Tembo et al. (1999), and magmatic units in the Mansa region from De Waele et al. (2006b).

Figure 9. Representative microphotographs of the studied Irumide samples. (A) Muscovite rims around deformed plagioclase and recrystallized quartz in the foliated monzogranite IR06 (XPL). (B) Biotite-rich zone in monzogranite IR07 where biotite reacts with iron oxide to from fine-grained white micas (PPL). (C) Intense alteration in andesite IR04, ex-hornblende reacts to oxides and a micaceous ground mass but preserves its characteristic cleavage (PPL). (D) Actinolite laths with pleochroitic halos around zircon or monazite inclusions in amphibolite IR05 (PPL). (E) Chalcopyrite mineralizations around quartz grains in the monzogranitic Mkushi complex IR11 (reflected light, PPL). (F) The Kapiri Mposhi Complex IR14 is nearly exclusively composed of quartz, partially sericitized feldspars and biotite (XPL). PPL, parallel polars; XPL, crossed polars; mineral abbreviations after Whitney and Evans (2010).

Figure 10. Representative microphotographs of the studied Bangweulu samples. (A) Intense deformation in Mansa monzogranite BG01 with fractured or mylonitized quartz and weathered, fractured and bended epidote (XPL). (B) K-feldspar porphyric texture in the eastern Bangweulu monzogranite BG18 (XPL). (C) Mansa metarhyolite BG07 contains intensely sericitized feldspars in a glass and mica-rich groundmass (XPL). (D) Mansa meta-andesite BG10 showing actinolite and epidote in a chlorite-feldspar-rich ground mass (XPL). PPL, parallel polars; XPL, crossed polars; mineral abbreviations after Whitney and Evans (2010).

Table 1

Table 1: Whole rock geochemistry of magmatic and metasedimentary rocks in the Domes, Bangweulu and Irumide regions.

DOMES		**Lumwana**						**Chimiwungo**						**Tshinsenda**		**Nchanga**	**Mufulira**			**Nkana**
ID		DO1	DO2	DO3	DO4	DO6	DO7	DO8	DO9	DO10	DO11	DO12	DO13	DO14	DO15	DO17	DO18	DO19	DO20	NSD49
Type[a]	**IDL**(wt. %, ppm)[b]	Amph	Gn	Gn	Gn	Gn	Gn/Mig	Gn/Mig	Gn/Mig	Gn	Gn/Sch	Gn/Sch	Gran	Gran	Gran	Gran	Gran	Sch	Sch	Sch
SiO_2	0.07	46.2	72.6	74.6	67.6	75.4	74.6	69.3	75.0	75.3	65.6	54.4	80.2	65.6	66.0	74.2	66.4	57.7	74.2	59.4
TiO_2	0.002	1.99	0.30	0.08	0.95	0.05	0.08	0.66	0.09	0.37	0.97	1.03	0.12	0.70	0.69	0.12	0.72	0.65	0.17	0.58
Al_2O_3	0.01	14.1	15.8	15.6	14.1	14.9	14.3	15.3	14.8	13.7	17.7	18.6	11.6	15.5	15.3	13.8	15.6	22.3	9.2	15.9
Fe_2O_{3T}	0.003	13.9	2.33	1.04	6.97	0.65	0.58	3.44	1.08	1.40	3.93	8.16	0.82	5.13	5.33	2.31	5.16	6.56	1.05	6.25
MnO	0.001	0.17	0.02	0.01	0.06	0.01	0.005	0.05	0.02	0.02	0.03	0.05	0.01	0.05	0.04	0.07	0.14	0.03	0.06	0.07
MgO	<0.001	7.68	0.85	0.31	3.14	0.30	0.22	0.49	0.17	0.24	1.44	6.36	0.07	1.85	1.88	0.06	1.47	2.61	0.71	3.94
CaO	0.002	9.54	2.10	2.37	1.30	1.68	0.68	1.12	1.23	1.49	3.44	2.21	0.45	2.59	2.51	1.07	3.50	0.12	4.10	1.01
Na_2O	0.01	2.67	4.87	5.03	2.60	5.46	3.06	4.36	5.65	3.61	5.26	3.37	2.87	2.97	2.95	3.43	3.58	0.46	0.85	0.50
K_2O	0.01	1.88	3.11	1.98	4.29	2.32	6.79	6.02	3.30	4.90	3.00	6.83	4.99	5.41	4.97	5.64	3.55	7.64	5.58	6.66
P_2O_5	0.01	0.38	0.05	0.02	0.16	0.01	b.l.	0.11	0.01	0.08	0.18	0.41	b.l.	0.20	0.21	0.01	0.25	0.08	0.05	0.23
Total		98.5	102.0	101.1	101.1	100.7	100.3	100.8	101.3	101.1	101.6	101.5	101.1	100.0	99.8	100.7	100.4	98.2	96.0	94.6
Ba	3.3	197	712	516	648	495	2250	1620	809	1310	923	1090	63	1880	1520	122	1420	1660	1160	1830
Sc	0.44	36.6	4.5	1.5	13.4	1.6	1.0	8.2	5.2	3.3	8.8	22.0	4.4	11.7	11.2	0.7	14.0	20.9	3.9	15.2
Sr	0.86	112	267	192	111	183	237	125	126	162	318	282	30	361	355	27	376	48	167	61
V	3.4	285	28.8	4.5	125	b.l.	6.2	11.1	b.l.	7.6	54.4	177	4.3	82.2	85.2	b.l.	61.9	122	13.3	105
Zn	25	81	b.l.	b.l.	38	b.l.	b.l.	34	b.l.	b.l.	b.l.	28	b.l.	b.l.	30	105	113	57	b.l.	50
Rb	*0.28*	*65.1*	*90.0*	*36.8*	*207*	*44.4*	*139*	*106*	*210*	*134*	*67.3*	*235*	*312*	*158*	*157*	*363*	*125*	*317*	*137*	*187*
Cs	*0.009*	*n.a.*	*1.18*	*n.a.*	*n.a.*	*n.a.*	*n.a.*	*n.a.*	*n.a.*	*n.a.*	*n.a.*	*n.a.*	*n.a.*	*n.a.*	*n.a.*	*n.a.*	*n.a.*	*n.a.*	*n.a.*	*n.a.*
Co	2	56	b.l.	b.l.	16	b.l.	b.l.	b.l.	b.l.	b.l.	11	44	b.l.	8	9	b.l.	b.l.	9	b.l.	186
Cr	12	238	66	296	38	35	14	68	36	38	48	28	6	167	196	b.l.	25	203	42	b.l.
Cu	14	16	b.l.	16	123	14	b.l.	b.l.	b.l.	b.l.	b.l.	b.l.	b.l.	b.l.	b.l.	b.l.	16	b.l.	b.l.	b.l.
Ni	10	90	11	b.l.	b.l.	b.l.	b.l.	b.l.	b.l.	b.l.	b.l.	42	b.l.	820	973	b.l.	b.l.	48	b.l.	b.l.
La	*0.16*	*24.5*	*8.62*	*12.0*	*53.6*	*3.56*	*3.18*	*65.8*	*132*	*85.4*	*67.6*	*43.0*	*619*	*33.7*	*37.1*	*62.2*	*58.5*	*57.8*	*18.3*	*8.60*
Ce	*0.52*	*54.2*	*18.3*	*23.8*	*105*	*6.88*	*10.1*	*130*	*260*	*164*	*138*	*93.1*	*466*	*76.6*	*76.7*	*135*	*94.5*	*104*	*37.2*	*17.7*
Pr	*0.08*	*7.33*	*2.47*	*2.96*	*12.3*	*0.85*	*0.89*	*16.5*	*32.9*	*19.7*	*17.9*	*12.4*	*50.3*	*6.86*	*6.86*	*17.8*	*10.0*	*12.67*	*4.89*	*2.23*
Nd	*0.29*	*31.9*	*9.38*	*11.7*	*46.0*	*3.42*	*3.49*	*66.6*	*131*	*72.7*	*73.5*	*52.3*	*134*	*26.2*	*25.3*	*71.7*	*35.3*	*47.5*	*19.0*	*9.07*
Sm	*0.048*	*7.47*	*1.92*	*2.44*	*9.37*	*0.79*	*0.81*	*13.3*	*27.2*	*15.4*	*15.4*	*11.3*	*17.8*	*5.65*	*5.03*	*24.4*	*5.8*	*8.93*	*3.96*	*2.09*
Eu	*0.008*	*2.01*	*0.76*	*0.89*	*1.14*	*0.42*	*0.95*	*3.39*	*6.81*	*2.35*	*5.39*	*2.1*	*2.6*	*1.64*	*1.49*	*0.76*	*1.83*	*1.74*	*0.78*	*0.6*
Gd	*0.032*	*6.84*	*1.23*	*1.54*	*7.02*	*0.64*	*0.5*	*9.95*	*19.7*	*13.0*	*11.8*	*8.38*	*13.8*	*4.43*	*4.14*	*26.1*	*4.14*	*5.97*	*2.83*	*1.77*
Tb	*0.005*	*1.26*	*0.19*	*0.22*	*1.18*	*0.1*	*0.08*	*1.66*	*3.32*	*2.5*	*2.02*	*1.35*	*2.16*	*0.78*	*0.77*	*5.78*	*0.66*	*0.92*	*0.46*	*0.31*
Dy	*0.032*	*7.03*	*0.89*	*0.79*	*5.37*	*0.5*	*0.39*	*8.22*	*16.4*	*14.2*	*10.28*	*6.3*	*9.67*	*4.21*	*4.21*	*37.56*	*3.06*	*3.83*	*2.1*	*1.7*
Ho	*0.005*	*1.57*	*0.18*	*0.13*	*1.01*	*0.1*	*0.08*	*1.74*	*3.53*	*3.17*	*2.22*	*1.23*	*2.09*	*0.94*	*0.96*	*8.93*	*0.67*	*0.7*	*0.44*	*0.4*
Y	*0.17*	*48.2*	*4.99*	*3.46*	*28.2*	*3.1*	*2.59*	*50.6*	*99.3*	*91.9*	*63.2*	*36.9*	*76.7*	*27.3*	*29.5*	*245*	*20.3*	*19.7*	*12.7*	*11.9*
Er	*0.028*	*4.48*	*0.48*	*0.28*	*2.51*	*0.28*	*0.25*	*4.89*	*9.72*	*9.44*	*6.15*	*3.15*	*5.8*	*2.78*	*2.82*	*26.8*	*1.88*	*1.74*	*1.26*	*1.24*
Tm	*0.005*	*0.62*	*0.07*	*0.03*	*0.33*	*0.05*	*0.04*	*0.68*	*1.35*	*1.39*	*0.84*	*0.41*	*0.85*	*0.39*	*0.42*	*3.78*	*0.27*	*0.23*	*0.19*	*0.2*
Yb	*0.047*	*4.24*	*0.52*	*0.19*	*2.22*	*0.40*	*0.36*	*4.56*	*9.26*	*9.37*	*5.71*	*2.71*	*6.53*	*2.78*	*2.99*	*23.62*	*1.88*	*1.61*	*1.41*	*1.35*
Lu	*0.005*	*0.62*	*0.09*	*0.03*	*0.33*	*0.08*	*0.06*	*0.66*	*1.3*	*1.32*	*0.84*	*0.38*	*1.02*	*0.43*	*0.46*	*3.13*	*0.3*	*0.24*	*0.23*	*0.2*
Zr	62	175	193	b.l.	396	84	b.l.	729	88	287	978	187	105	240	263	189	207	98	b.l.	173
Nb	*0.11*	*16.8*	*8.0*	*2.6*	*21.1*	*3.7*	*2.1*	*10.6*	*20.9*	*28.4*	*4.9*	*13.3*	*17.0*	*11.1*	*11.6*	*84.3*	*15.6*	*8.7*	*5.7*	*10.0*
Ta	*0.053*	*1.3*	*b.l.*	*b.l.*	*1.2*	*0.5*	*b.l.*	*0.9*	*1.5*	*0.5*	*b.l.*	*0.8*	*b.l.*	*0.6*	*0.9*	*2.7*	*0.6*	*b.l.*	*0.5*	*1.0*
Th	*0.090*	*4.3*	*5.1*	*5.8*	*25.9*	*5.2*	*2.1*	*9.8*	*19.5*	*22.8*	*8.9*	*2.5*	*71.4*	*8.6*	*8.6*	*90.8*	*10.9*	*17.3*	*5.7*	*10.0*
U	*0.006*	*1.2*	*0.6*	*0.8*	*2.5*	*1.9*	*0.5*	*2.7*	*5.5*	*5.4*	*4.5*	*4.8*	*3.1*	*2.4*	*2.6*	*12.6*	*1.6*	*1.5*	*0.8*	*2.3*
Pb	*0.32*	*3.3*	*9.0*	*11.3*	*4.9*	*10.9*	*12.6*	*28.4*	*57.8*	*19.8*	*3.5*	*1.9*	*27.9*	*3.8*	*3.5*	*64.1*	*14.1*	*11.2*	*5.1*	*1.0*

Table 1(continued).

BANGWEULU				**Mansa region (SW Bangweulu)**										**South-Central to West Bangweulu**					
ID		BGA	BGQ	BG01	BG02	BG03	BG07	BG08	BG09	BG10	BG04	BG05	BG06	BG11	BG13	BG14	BG15	BG17	BG18
Type[a]	**IDL**(wt. %, ppm)[b]	Gran	Qzte	Gran	Gran	Q-lat	Rhyol	Q-lat	AF rhyol	And	Qzte	Siltst	Qzite	Qzte	Gran	Siltst	Siltst	Clayst	Gran
SiO_2	0.07	71.2	80.5	71.9	74.0	66.5	70.3	66.7	69.2	60.1	94.7	101.4	72.8	98.2	72.6	65.6	66.9	37.2	75.3
TiO_2	0.002	0.56	0.52	0.54	0.29	0.63	0.42	0.49	0.52	0.78	0.09	0.03	0.46	0.03	0.39	0.64	0.71	0.9	0.2
Al_2O_3	0.01	14.0	9.9	14.0	14.4	17.5	16.0	17.9	17.9	19.5	1.1	0.2	14.7	0.7	13.7	20.4	19.3	19.2	14.0
Fe_2O_{3T}	0.003	3.41	2.91	2.97	1.76	4.08	1.92	2.83	3.07	4.58	0.99	0.07	5.92	0.08	2.28	2.81	5.69	31.0	1.65
MnO	0.001	0.06	0.04	0.06	0.05	0.09	0.05	0.07	0.14	0.21	b.l.	b.l.	0.004	b.l.	0.03	0.004	0.001	0.01	0.05
MgO	<0.001	0.84	0.91	0.79	0.43	1.33	0.42	0.68	0.47	1.44	0.03	0.01	0.35	0.01	0.56	0.42	0.28	0.53	0.46
CaO	0.002	1.62	0.87	2.1	1.29	1.83	1.7	2.94	0.04	4.3	0.01	0.01	0.03	b.l.	0.6	0.01	0.01	0.04	0.43
Na_2O	0.01	3.27	2.78	3.02	3.47	4.43	4.22	4.1	0.25	4.08	b.l.	0.01	0.08	b.l.	2.01	0.09	0.12	0.07	2.59
K_2O	0.01	5.53	2.73	4.53	5.06	4.7	4.58	5.18	6.43	4.84	0.19	0.04	4.38	0.18	6.15	6.64	5.24	4.6	5.24
P_2O_5	0.01	0.17	0.12	0.15	0.06	0.2	0.12	0.13	0.12	0.24	b.l.	0.01	0.06	b.l.	0.13	0.08	0.06	0.18	0.19
Total		100.7	101.2	100.1	100.8	101.3	99.8	101.0	98.2	100.0	97.2	101.7	98.8	99.2	98.4	96.7	98.3	93.7	100.1
Ba	3.3	1970	507	1040	1330	1950	2840	3280	2730	2580	37	12	640	18	508	623	744	450	280
Sc	0.44	4.2	5.8	5.9	3.8	7.2	4.9	6.3	6.9	7.6	0.9	b.l.	9.3	b.l.	5.9	17.5	12.2	14.4	6.7
Sr	0.86	326	106	267	205	441	407	572	95	772	2	6	33	7	72	104	77	15	57
V	3.4	29.8	50.2	45	20	64	32	33	35	72	9	b.l.	56	4	19	94	71	183	10
Zn	25	57	b.l.	29	35	76	40	52	98	102	b.l.	b.l.	8	b.l.	b.l.	b.l.	b.l.	31	33
Ga	18	b.l.	b.l.	b.l.	22	b.l.	20	18	b.l.	22	b.l.	b.l.	25	b.l.	18	28	25	38	18
Rb	*0.28*	*144*	*58.9*	*203*	*171*	*144*	*128*	*118*	*311*	*140*	*11.61*	*0.88*	*146*	*10.2*	*339*	*436*	*199*	*213*	*282*
Cs	*0.009*	*n.a.*	*n.a.*	*4*	*1.98*	*2.93*	*2.77*	*2.41*	*5.61*	*2.58*	*0.34*	*0.09*	*3.89*	*0.17*	*2.29*	*6.56*	*3.42*	*9.38*	*13.7*
Co	2	b.l.	b.l.	b.l.	b.l.	3	b.l.	b.l.	b.l.	4	b.l.	b.l.	b.l.	b.l.	b.l.	b.l.	b.l.	8	b.l.
Cr	12	34	105	b.l.	35	b.l.	b.l.	47	b.l.	27	33	b.l.	b.l.	b.l.	b.l.	32	b.l.	265	b.l.
Cu	14	b.l.	b.l.	b.l.	b.l.	b.l.	b.l.	b.l.	b.l.	14	b.l.	b.l.	b.l.	b.l.	b.l.	b.l.	b.l.	b.l.	b.l.
Ni	10	b.l.	b.l.	b.l.	b.l.	b.l.	b.l.	b.l.	b.l.	b.l.	b.l.	b.l.	b.l.	b.l.	b.l.	b.l.	b.l.	b.l.	b.l.
La	*0.16*	*202*	*23.0*	*55.3*	*63.3*	*53.8*	*54.8*	*59.3*	*115*	*54.4*	*9.44*	*7.06*	*49.8*	*8.32*	*96.4*	*114*	*86.8*	*15.4*	*17.2*
Ce	*0.52*	*349*	*47.7*	*99.4*	*98.1*	*95.5*	*99.3*	*107*	*92.3*	*103*	*23.0*	*13.5*	*96.1*	*15.3*	*282*	*166*	*152*	*28.8*	*40.1*
Pr	*0.08*	*32.0*	*5.85*	*11.7*	*10.9*	*11.2*	*10.9*	*11.7*	*28.6*	*11.8*	*2.56*	*1.52*	*11.5*	*1.72*	*27.6*	*20.9*	*17.9*	*2.48*	*4.31*
Nd	*0.29*	*112*	*22.9*	*42.3*	*38.7*	*40.8*	*38.8*	*42.1*	*102*	*43.8*	*9.75*	*5.7*	*42.4*	*6.01*	*107*	*66.9*	*61.9*	*8.4*	*16.2*
Sm	*0.048*	*16.5*	*4.50*	*7.6*	*7.13*	*7.05*	*6.23*	*6.96*	*15.0*	*7.66*	*1.95*	*1.23*	*6.76*	*1.1*	*22.8*	*10.9*	*10.5*	*1.71*	*4.32*
Eu	*0.008*	*3.22*	*0.89*	*1.54*	*1.53*	*1.98*	*1.78*	*2.35*	*2.86*	*2.36*	*0.34*	*0.23*	*0.97*	*0.11*	*1.22*	*1.8*	*1.92*	*0.49*	*0.41*
Gd	*0.032*	*10.5*	*3.33*	*6.78*	*7.05*	*5.42*	*4.59*	*5.05*	*9.22*	*5.7*	*1.21*	*1.85*	*4.55*	*0.69*	*15.3*	*7.31*	*5.62*	*2.1*	*4.23*
Tb	*0.005*	*1.52*	*0.47*	*1.19*	*1.21*	*0.89*	*0.75*	*0.81*	*1.43*	*0.93*	*0.17*	*0.38*	*0.81*	*0.1*	*2.33*	*1.09*	*0.78*	*0.46*	*0.87*
Dy	*0.032*	*8.69*	*2.44*	*5.95*	*6.21*	*3.93*	*3.29*	*3.46*	*5.42*	*4.08*	*0.62*	*1.81*	*3.92*	*0.37*	*8.74*	*3.53*	*3.05*	*2.64*	*4.57*
Ho	*0.005*	*1.75*	*0.43*	*1.45*	*1.47*	*0.86*	*0.72*	*0.75*	*1.04*	*0.89*	*0.14*	*0.34*	*0.93*	*0.08*	*1.54*	*0.61*	*0.7*	*0.63*	*0.96*
Y	*0.17*	*47.3*	*10.7*	*45.7*	*52.9*	*26.6*	*21.5*	*22.0*	*27.2*	*26.7*	*3.18*	*10.4*	*26.8*	*2.12*	*43.5*	*15.4*	*20.4*	*17.7*	*30.2*
Er	*0.028*	*4.98*	*1.14*	*4.11*	*4.27*	*2.45*	*2.08*	*2.12*	*2.86*	*2.52*	*0.41*	*0.83*	*2.83*	*0.21*	*3.58*	*1.57*	*2.23*	*1.92*	*2.72*
Tm	*0.005*	*0.75*	*0.17*	*0.58*	*0.6*	*0.34*	*0.31*	*0.31*	*0.41*	*0.36*	*0.07*	*0.1*	*0.43*	*0.03*	*0.43*	*0.22*	*0.36*	*0.29*	*0.4*
Yb	*0.047*	*4.85*	*1.07*	*3.93*	*4.05*	*2.43*	*2.26*	*2.25*	*3.04*	*2.59*	*0.5*	*0.68*	*3.22*	*0.26*	*2.66*	*1.73*	*2.8*	*2.21*	*2.88*
Lu	*0.005*	*0.72*	*0.17*	*0.59*	*0.62*	*0.38*	*0.36*	*0.36*	*0.47*	*0.41*	*0.08*	*0.09*	*0.5*	*0.04*	*0.38*	*0.28*	*0.44*	*0.33*	*0.41*
Zr	62/2.3	362	195	*141*	*141*	*252*	*246*	*307*	*243*	*379*	*72.2*	*27.9*	*177*	*42.5*	*305*	*183*	*255*	*289*	*117*
Hf	*0.12*	*5.52*	*2.79*	*4.65*	*4.81*	*6.93*	*7.28*	*8.35*	*7.6*	*9.88*	*2.13*	*0.87*	*5.58*	*1.39*	*9.82*	*5.93*	*7.8*	*8.74*	*4.07*
Nb	*0.11*	*n.a.*	*n.a.*	*26.1*	*19.4*	*7.2*	*18.7*	*17.9*	*27.7*	*24.4*	*2.7*	*0.8*	*17.4*	*3.3*	*35.7*	*24.1*	*22.4*	*27.5*	*24.3*
Ta	*0.053*	*n.a.*	*n.a.*	*1.09*	*0.98*	*0.16*	*1.37*	*1.03*	*2.15*	*1.49*	*0.21*	*b.l.*	*1.33*	*0.32*	*1.28*	*1.45*	*1.46*	*2.1*	*2.35*
Th	*0.090*	*n.a.*	*n.a.*	*21.2*	*15.7*	*15.0*	*14.0*	*13.1*	*17.3*	*15.4*	*3.38*	*2.06*	*15.3*	*9.56*	*117*	*21.2*	*19.5*	*27.6*	*13.1*
U	*0.006*	*n.a.*	*n.a.*	*4.77*	*3.12*	*2.76*	*2.87*	*2.35*	*4.54*	*2.57*	*0.33*	*0.26*	*2.35*	*0.25*	*3.31*	*2.62*	*2.86*	*4.19*	*5.9*
Pb	*0.32*	*n.a.*	*n.a.*	*18.8*	*19.1*	*8.64*	*26.6*	*31.6*	*16.4*	*73.3*	*2.13*	*2.06*	*6.97*	*1.13*	*69.7*	*6.3*	*8.48*	*15.9*	*21.7*

Table 1(continued).

IRUMIDE		**NE Irumide**				**Central Irumide**			**SW Irumide**			
ID		IR01	IR02	IR03	IR04	IR05	IR06	IR07	IR09	IR10	IR13	IR14
Type[a]	**IDL**(wt. %, ppm)[b]	Qzte	Siltst	Siltst	And	Amph	Gran	Gn	Sch	Phyll	Gran	Gran
SiO_2	0.07	100.6	66.3	60.5	50.5	48.2	78.9	83.6	69.4	55.6	75.7	71.5
TiO_2	0.002	0.02	0.87	0.93	0.73	1.99	0.32	0.19	1.07	1.08	0.3	0.31
Al_2O_3	0.01	0.3	17.6	18.4	18.6	15.9	12.0	10.0	23.8	24.1	13.8	15.0
Fe_2O_{3T}	0.003	0.01	8.76	12.04	10	14.34	3.03	2.21	0.76	6.4	2.03	2.49
MnO	0.001	b.l.	0.004	0.57	0.16	0.19	0.1	0.04	b.l.	0.02	0.06	0.04
MgO	<0.001	0.01	0.12	1.59	6.38	7.79	0.69	0.08	0.18	0.18	0.51	0.73
CaO	0.002	0.01	0.05	0.1	11.4	9.16	0.97	0.77	b.l.	0.07	1.23	2.56
Na_2O	0.01	b.l.	0.43	0.43	2.14	2.69	2.3	1.77	0.23	0.68	2.88	4.07
K_2O	0.01	0.08	3.44	4.96	1.03	0.09	4.35	4.81	3.6	4.86	5.1	2.46
P_2O_5	0.01	b.l.	0.03	0.11	0.08	0.28	0.19	0.02	0.05	0.05	0.06	0.08
Total		101.0	97.6	99.6	101.0	100.7	102.9	103.4	99.1	93.1	101.7	99.3
Ba	3.3	13	682	2980	334	67	333	278	349	851	512	633
Sc	0.44	b.l.	12.7	16.3	32.4	21.8	5.7	7	14.1	15.2	6.3	3.4
Sr	0.86	1	63	86	185	219	50	27	120	78	78	260
V	3.4	b.l.	66	113	204	249	23	b.l.	124	64	22	24
Zn	25	b.l.	b.l.	87	77	131	83	57	b.l.	523	32	58
Ga	18	b.l.	25	25	22	19	34	19	33	37	b.l.	21
Rb	*0.28*	*2*	*179*	*256*	*32*	*2*	*416*	*179*	*123*	*310*	*290*	*83*
Cs	*0.009*	*0.06*	*8.5*	*13.4*	*0.34*	*0.58*	*37.4*	*n.a.*	*17.7*	*13.0*	*5.67*	*1.81*
Co	2	b.l.	5	51	44	71	b.l.	b.l.	b.l.	4	b.l.	b.l.
Cr	12	b.l.	b.l.	70	121	103	b.l.	b.l.	60	21	b.l.	b.l.
Cu	14	b.l.	b.l.	b.l.	77	25	b.l.	b.l.	b.l.	b.l.	b.l.	b.l.
Ni	10	b.l.	b.l.	11	41	160	b.l.	b.l.	b.l.	b.l.	b.l.	b.l.
La	*0.16*	*1.57*	*4.15*	*56.7*	*11.7*	*13.8*	*78.6*	*n.a.*	*56.1*	*21.2*	*33*	*35.1*
Ce	*0.52*	*2.46*	*7.3*	*121*	*22.0*	*28.1*	*139*	*n.a.*	*104*	*35.5*	*81.2*	*58.2*
Pr	*0.08*	*0.27*	*0.67*	*11.7*	*2.68*	*3.74*	*15.2*	*n.a.*	*11.7*	*4.1*	*8.93*	*6.36*
Nd	*0.29*	*1*	*2.92*	*42.5*	*11.3*	*16.7*	*52.3*	*n.a.*	*41.3*	*15.3*	*32.6*	*21.8*
Sm	*0.048*	*0.25*	*0.9*	*7.9*	*2.86*	*4.21*	*9.96*	*n.a.*	*7.54*	*3.33*	*6.95*	*3.55*
Eu	*0.008*	*0.04*	*0.3*	*1.93*	*0.96*	*1.63*	*0.62*	*n.a.*	*1.31*	*0.79*	*0.93*	*0.79*
Gd	*0.032*	*0.3*	*1.22*	*6.38*	*3.19*	*4.46*	*7.89*	*n.a.*	*4.85*	*3.25*	*5.67*	*2.59*
Tb	*0.005*	*0.05*	*0.28*	*1.09*	*0.61*	*0.81*	*1.39*	*n.a.*	*0.72*	*0.63*	*1.07*	*0.4*
Dy	*0.032*	*0.24*	*1.81*	*5.07*	*3.42*	*4.31*	*6.29*	*n.a.*	*2.54*	*3.47*	*5.31*	*1.5*
Ho	*0.005*	*0.06*	*0.46*	*1.17*	*0.8*	*0.98*	*1.32*	*n.a.*	*0.49*	*0.8*	*1.16*	*0.29*
Y	*0.17*	*1.54*	*13.5*	*37.3*	*22.8*	*28.2*	*40.9*	*55.6*	*12.9*	*21.3*	*35.2*	*9.92*
Er	*0.028*	*0.15*	*1.53*	*3.43*	*2.27*	*2.79*	*3.72*	*n.a.*	*1.35*	*2.48*	*3.47*	*0.76*
Tm	*0.005*	*0.02*	*0.26*	*0.49*	*0.32*	*0.38*	*0.53*	*n.a.*	*0.2*	*0.38*	*0.52*	*0.09*
Yb	*0.047*	*0.16*	*2.11*	*3.49*	*2.19*	*2.63*	*3.7*	*n.a.*	*1.56*	*2.72*	*3.71*	*0.6*
Lu	*0.005*	*0.02*	*0.34*	*0.53*	*0.32*	*0.38*	*0.54*	*n.a.*	*0.25*	*0.41*	*0.53*	*0.09*
Zr	*2.3*	*20.5*	*393*	*212*	*95*	*89*	*219*	*238*	*1250*	*228*	*161*	*171*
Hf	*0.12*	*0.74*	*11.8*	*6.1*	*2.86*	*2.46*	*8.12*	*n.a.*	*14.2*	*7.23*	*5.56*	*4.9*
Nb	*0.11*	*0.46*	*26.1*	*32.7*	*7.58*	*1.85*	*38.3*	*n.a.*	*20.8*	*12.3*	*21.9*	*8.14*
Ta	*0.053*	*0.05*	*1.17*	*0.87*	*0.47*	*0.1*	*1.54*	*n.a.*	*1.35*	*1.17*	*0.8*	*0.9*
Th	*0.090*	*0.82*	*23.9*	*19.6*	*2.47*	*1.88*	*51.0*	*n.a.*	*26.3*	*33.4*	*37.5*	*23.2*
U	*0.006*	*0.2*	*1.91*	*2.58*	*0.39*	*0.19*	*8.11*	*n.a.*	*3.84*	*3.74*	*3.87*	*1.57*
Pb	*0.32*	*1.24*	*21.0*	*24.7*	*8.48*	*30.7*	*46.4*	*b.l.*	*11.7*	*58.5*	*37.6*	*15.3*

[a] Clayst, claystone; Siltst, siltstone; Sandst, sandstone; Phyll, phyllite; Sch, schist; Qzte, quartzite; Gn, gneiss; Mig, migmatite; Amph, amphibolite; Gran, granitoid; Rhyol, rhyolite; AF rhyol, alkali feldspar rhyolite; Q lat, quartz latite; And, andesite; Dol, dolerite.

[b] Concentrations and instrumental detection limits (IDL) for ICP-OES (normal) and ICP-MS data (italic); b.l., below limit; n.a., not analyzed.

Table 2

Table 2. Whole rock Sm-Nd isotope data for igneous and sedimentary rocks in the Domes, Bangweulu and Irumide regions.

Domes	Type	ID	T (Ga)[a]	$^{143}Nd/^{144}Nd$	2s	$^{147}Sm/^{144}Nd$	1s(rel)	T_{DM}(Ga)	εNd (now)	εNd (T)
Magm.	Amph	DO11JV001	1.50	0.51200	0.00005	0.142	0.02	2.22±0.11	-13	-2
	Grt	DO11JV013	1.92	0.51135	0.00004	0.080	0.02	1.93±0.03	-25	4
	Grt	DO11JV014	1.92	0.51165	0.00006	0.130	0.02	2.57±0.10	-19	-3
	Grt	DO11JV015	1.92	0.51158	0.00005	0.120	0.02	2.40±0.08	-21	-2
	Grt	DO11JV017	0.88	0.51205	0.00007	0.205	0.02	N.A.[b]	-11	-12
	Grt	DO11JV018	1.95	0.51118	0.00005	0.099	0.02	2.49±0.06	-28	-4
Orthogn?	Gn	DO11JV007	1.92	0.51159	0.00006	0.140	0.02	3.07±0.14	-20	-7
	Gn	DO11JV008	1.92	0.51168	0.00005	0.121	0.02	2.24±0.07	-19	0
	Gn	DO11JV010	1.92	0.51158	0.00005	0.128	0.02	2.63±0.09	-21	-4
Metased	Luf S	DO11JV019	1.95	0.51131	0.00005	0.114	0.02	2.66±0.08	-26	-5
	Luf S	DO11JV020	1.95	0.51160	0.00005	0.126	0.02	2.52±0.09	-20	-2
	Luf S	NS12DD49	1.92	0.51155	0.00006	0.139	0.02	3.11±0.14	-21	-7
	Gn	DO11JV002	1.92	0.51164	0.00006	0.124	0.02	2.38±0.09	-19	-1
	Gn	DO11JV003	1.92	0.51162	0.00005	0.127	0.02	2.50±0.09	-20	-3
	Gn	DO11JV004	1.92	0.51162	0.00006	0.123	0.02	2.40±0.08	-20	-2
	Gn	DO11JV006	1.92	0.51168	0.00005	0.140	0.02	2.83±0.13	-19	-5
	Gn/sch	DO11JV011	1.92	0.51169	0.00004	0.127	0.02	2.37±0.08	-18	-1
	Gn/sch	DO11JV012	1.92	0.51169	0.00006	0.130	0.02	2.48±0.10	-19	-2
Bangweulu and Irumide										
Magm.	Gran	BG12JV01	1.87	0.51146	0.00006	0.109	0.02	2.30±0.07	-23	-2
	Gran	BG12JV01	1.87	0.51150	0.00007	0.109	0.02	2.24±0.07	-22	-1
	Gran	BG12JV02	1.87	0.51140	0.00007	0.111	0.02	2.47±0.08	-24	-4
	Extr	BG12JV03	1.87	0.51142	0.00006	0.104	0.02	2.27±0.06	-24	-2
	Extr	BG12JV07	1.87	0.51127	0.00006	0.097	0.02	2.30±0.06	-27	-3
	Extr	BG12JV08	1.87	0.51133	0.00004	0.100	0.02	2.30±0.05	-26	-2
	Extr	BG12JV09	1.87	0.51145	0.00007	0.089	0.02	1.94±0.05	-23	3
	Extr	BG12JV10	1.87	0.51139	0.00006	0.106	0.02	2.34±0.07	-24	-3
	Gran	BG12JV12	1.96	0.51148	0.00006	0.136	0.02	3.14±0.36	-23	-8
	Migm	BG12JV13	1.96	0.51146	0.00006	0.129	0.02	2.88±0.11	-23	-6
	Gran	BG12JV18	1.96	0.51183	0.00005	0.161	0.02	3.62±0.27	-16	-7
	Maf	IR12JV04	1.96	0.51183	0.00006	0.153	0.02	3.08±0.19	-16	-5
	Maf	IR12JV05	1.96	0.51205	0.00006	0.153	0.02	2.50±0.15	-12	0
	Gran	IR12JV06	1	0.51112	0.00005	0.115	0.02	3.01±0.08	-30	-19
	Gran	IR12JV13	1	0.51143	0.00007	0.129	0.02	2.93±0.11	-24	-15
	Gran	IR12JV14	2.74	0.51085	0.00006	0.098	0.02	2.93±0.07	-35	0
Sed.	Sed	BG12JV06	1.8	0.51138	0.00008	0.096	0.02	2.16±0.07	-25	-1
	Sed	BG12JV14	1.8	0.51158	0.00005	0.098	0.02	1.93±0.05	-21	2
	Sed	BG12JV15	1.8	0.51151	0.00005	0.102	0.02	2.10±0.05	-22	0
	Sed	BG12JV17	1.8	0.51149	0.00005	0.123	0.02	2.64±0.09	-22	-5
	Sed	IR12JV02	1.8	0.51146	0.00005	0.186	0.02	N.A.[b]	-23	-21
	Sed	IR12JV03	1.8	0.51147	0.00006	0.112	0.02	2.36±0.07	-23	-3
	Sed	IR12JV09	1.8	0.51134	0.00006	0.110	0.02	2.53±0.07	-25	-5
	Sed	IR12JV10	1.8	0.51136	0.00006	0.132	0.02	3.19±0.13	-25	-10

[a] The chosen age T for the undated Domes units is 1.92 Ga, the central value of the igneous Domes ages referenced in the text (1.98-1.86 Ga). This corresponds closely to the 1.91 Ga modus of igeous zircon ages by Eglinger (2013). Bangweulu and Irumide ages follow the central values from the corresponding magmatic phase of De Waele et al. (2006b) and references therein. The isotope composition of the Muva Supergroup and inferred correlatives is shown at the inferred depositional age of the former (~1.8 Ga, De Waele and Fitzsimons, 2007). [b] N.A., not applicable.

Table A

Table A. Macroscopic description and available GPS coordinates (in WGS84) of the studied samples.

Sample	Macroscopic description	Drill Core/Location	Depth	RMCA
DO11JV01	Medium-grained (3mm) amphibolite schist with lineated amphiboles and feldspar-filled veinlets	LUB0220[a]	51 m	-
DO11JV02	Medium-grained (2-3mm), heterogenic, white granitoid biotite gneiss	LUB0220	59.5 m	-
DO11JV03	Medium-grained (2-3mm), heterogenic, white granitoid biotite gneiss, fewer biotite than DO02	LUB0220	88.5 m	-
DO11JV05	Medium-grained (2-3mm), heterogenic, white granitoid biotite gneiss, fewer biotite than DO02	LUB0220	88.5 m	-
DO11JV06	Medium-grained (2-3mm) , white granitoid gneiss	LUB0220	125.5 m	-
DO11JV07	Coarse-grained, pegmatoidal, pinkish granitoid biotite gneiss with biotite-annealed fractures, feldspars up to 1cm	LUB0220	35.5 m	-
DO11JV08	Coarse-grained (5mm) pinkish granitoid biotite gneiss with quartz veins	CHI00707[b]	262.5 m	-
DO11JV09	Coarse-grained gneiss with a pinkish, heterogenic felsic pegmatoid part & homogeneous, banded mafic/felsic part (cf. DO10) feldspars up to 4cm	CHI00707	269 m	-
DO11JV10	Medium-grained (3mm) pinkish granitoid gneiss + quartz-biotite-rich bands and quartz veins	CHI00707	288 m	-
DO11JV11	Medium-grained (3mm), homogeneous white gneiss, with schistose quartz biotite dominated parts	CHI00707	509 m	-
DO11JV12	Medium-grained (3mm), white granitoid biotite gneiss with abundant biotite dominated schistose parts and coarse-grained (<1cm) heterogenic felsic parts	CHI00707	502 m	-
DO11JV13	Medium-grained (2-3mm) homogeneous, biotite granite, no banding, foliated, weathered appearance	Lumwana[c]	0 m	-
DO11JV14	Granitoid, powdered sample	Tshinsenda	-	R.G.71.282
DO11JV15	Medium-grained (2mm) titanite-rich epidote granitoid sample, feldspars up to 8mm	Tshinsenda	-	R.G.71.286
DO11JV16	Medium-grained (2mm) biotite-chlorite granitoid	-	-	R.G.71.291
DO11JV17	Medium- to coarse-grained, pink biotite granitoid	Nchanga	-	R.G.71.190
DO11JV18	Medium-grained (2mm), grey, titanite-rich biotite-epidote granite	Mufulira	-	R.G.70.552
DO11JV19	Dark green, fine-grained chlorite-tourmaline schist	Mufulira	-	R.G.70.553
DO11JV20	Pale green, fine-grained, banded chlorite-bearing quartz schist	Mufulira	960 m	-
NS12DD49	Pale green fine-grained, mottled chlorite-feldspar-quartz schist	SE797[d]	48-98 m	-

Sample number format and representative grain sizes are indicated between brackets. Abbreviations: DO, Domes region; IR, Irumide region; BG, Bangweulu region. The RMCA numbers refer to the collection numbers from the Royal Museum for Central Africa in Tervuren, Brussels; sample IDs refer to the KUL collection numbers. The latter are abbreviated in other sections. [a]LUB0220: S12 8.968 E25 57.300 (WGS84); [b]CHI00707: S12 16.921 E25 51.642 (WGS84);[c] S12 16.291 E25 40.141 [d] Nkana South copper mine, Kitwe, Zambia.

Table A(continued).

Sample ID	Macroscopic description	Stratigraphy	GPS coordinates/RMCA
IR12JV01	Massive, fine-grained (<1mm) white quartzite	Manshya River Gr	S11 37.380 E31 31.638 1620 m
IR12JV03	Black-blue siltstone showing fissibility	Manshya River Gr	S11 42.430 E31 35.208 1514 m
IR12JV04	Plagioclase-pyroxene-amphibole phenocrystic (2-3mm) metavolcanite with micaceous matrix	n.a.	S11 55.480 E31 32.378 1389 m
IR12JV05	Fine-grained (<1mm), massive dark grey homogeneous, amphibolite	n.a.	S11 55.595 E31 32.705 1353 m
IR12JV06	Medium- to coarse-grained (1-5mm), foliated, white, biotite granitoid, contains biotite-quartz dominated zones in outcrop	n.a.	S12 17.232 E31 06.345 1479 m
IR12JV07	Coarse-grained (3-5mm) white to pinkish biotite granitoid	n.a.	S12 40.353 E31 01.353 1578 m
IR12JV08	Sugar-textured white sandstone, rimmed by black crust	Kanona Gr	S13 03.675 E30 38.698 1645 m
IR12JV09	White-green to golden, micaceous quartzitic schist	Kanona Gr	S13 04.692 E30 36.312 1649 m
IR12JV10	Purple-red micaceous phyllite	Kanona Gr	S13 40.805 E29 15.861 1255 m
IR12JV11[d]	Chalcopyrite and malachite mineralized white to pink granitoid	n.a.	S13 56.919 E29 08.569 1134 m
IR12JV12[d]	Chalcopyrite and malachite mineralized whitish to beige granitoid	n.a.	S13 56.919 E29 08.569 1134 m
IR12JV13	Medium- to coarse-grained (2mm), feldspar porphyric (<4mm) biotite granitoid	n.a.	S13 56.661 E29 08.920 1155 m
IR12JV14	Fine-grained (1-2mm), homogeneous, white-greenish biotite granodiorite	n.a.	S13 45.318 E28 40.261 1232 m
BG11JV001	Coarse-grained (3-4mm) dark red equigranular biotite granitoid (BGA)	n.a.	R.G.42.282
BG11JV002	Sugar textured massive quartzite (Kamuzua basement quartzite of N. Zambia, BGQ)	Muva S-Gr	R.G.70.638
BG12JV01	Coarse-grained, equigranular (3-5mm), foliated, greenish, biotite granitoid with epidote and titanite	n.a.	S11 18.647 E28 51.475 1243 m
BG12JV02	Medium-grained (2mm), equigranular, reddish, chlorite-biotite-epidote granitoid	n.a.	S11 11.534 E28 45.136 1241 m
BG12JV03	Fine-grained, massive, feldspar and quartz phenocrystic metavolcanite with dark grey matrix	n.a.	S11 11.113 E28 40.684 1120 m
BG12JV04	Massive, fine-grained (< 1mm), equigranular, sugar-textured quartzite	Nsama Fm	S10 56.802 E28 48.940 1280 m
BG12JV05	Fine-grained (<1mm) equigranular, pinkish quartzite	Kabweluma Fm	S10 54.865 E28 48.403 1308 m
BG12JV06	Banded red siltstone without fissibility	Nsama Fm	S10 54.957 E28 48.347 1317 m
BG12JV07	Quartz and red feldspar phenocrystic metavolcanite with black miceaceous matrix	n.a.	S10 59.178 E28 49.850 1320 m
BG12JV08	Plagioclase phenocrystic (1-2mm) metavolcanite with greenish chlorite matrix	n.a.	S11 00.571 E28 50.015 1294 m
BG12JV09	Feldspar phenocrystic, red metavolcanite with Mn-oxides in veinlets	n.a.	S11 00.448 E28 48.664 1305 m
BG12JV10	Massive, amphibole phenocrystic metavolcanite with chlorite-rich matrix	n.a.	S11 06.416 E28 52.625 1254 m
BG12JV11	Massive, sugar-textured, pink quartzite with minor opaques	(Nsama Fm)	S10 50.156 E29 01.874 1285 m
BG12JV12	Coarse-grained (3-4mm) greenish epidote-(amphibole) granitoid with muscovite filling veinlets	n.a.	S10 12.788 E30 10.099 1346 m
BG12JV13	Coarse-grained (3-4mm) greenish epidote-(amphibole) granitoid with well developed shear planes and decimeter to meter-scaled quartz veins	n.a.	S10 13.153 E30 11.944 1285 m
BG12JV14	Massive white to reddish siltstone	(Nsama Fm)	S10 14.104 E30 24.022 1455 m
BG12JV15	Micaceous red siltstone	(Nsama Fm)	S10 19.139 E30 46.698 1412 m
BG12JV16	Red-black quartzite with biotite spots, weathered along stratification	Kasama Fm	S10 12.932 E31 09.025 1381 m
BG12JV17	Dark-red fine-grained argillite, with fissibility evolving to slatey cleavage	Kasama Fm	S10 09.666 E31 01.117 1354 m
BG12JV18	Coarse-grained (2-5mm), homogeneous, white-green epidote granitoid	n.a.	S10 16.827 E31 05.727 1270 m

[d]Seringa mining Ltd/Mkushi Copper joint venture

Table B. Whole rock Rb-Sr isotope data for igneous and sedimentary rocks in the Domes, Bangweulu and Irumide regions.

Domes	Type	ID	T (Ga)[a]	$^{87}Sr/^{86}Sr$	2s	$^{87}Rb/^{86}Sr$	Sr(T)
Magmatics	Amph	DO11JV001	1.50	0.74706	0.00017	1.22	0.72082
	LEG	DO11JV013	1.92	1.27363	0.00046	49.4	-
	Grt	DO11JV014	1.92	0.73328	0.00028	1.32	0.69680
	Grt	DO11JV015	1.92	0.73294	0.00019	1.31	0.69687
	NG	DO11JV017	0.88	1.18962	0.00051	42.4	0.65689
	MGG	DO11JV018	1.95	0.73461	0.00031	0.94	0.70813
Orthogn.?	Gn	DO11JV007	1.92	0.74005	0.00022	1.75	0.69183
	Gn	DO11JV008	1.92	0.76101	0.00019	2.47	0.69283
	Gn	DO11JV010	1.92	0.77199	0.00020	2.60	0.70028
Metasediments	Luf S	DO11JV019	1.95	1.07431	0.00081	21.9	0.45938
	Luf S	DO11JV020	1.95	0.75021	0.00022	2.36	0.68398
	Luf S	NS12DD49	1.92	0.78267	0.00008	9.0	0.53409
	Gn	DO11JV002	1.92	0.72989	0.00031	0.99	0.70251
	Gn	DO11JV003	1.92	0.74175	0.00025	0.61	0.72498
	Gn	DO11JV004	1.92	0.78653	0.00031	5.7	0.62891
	Gn	DO11JV006	1.92	0.73711	0.00037	0.75	0.71643
	Gn/sch	DO11JV011	1.92	0.72312	0.00018	0.65	0.70507
	Gn/sch	DO11JV012	1.92	0.73920	0.00030	2.53	0.66921
Bangweulu and Irumide							
Magmatics	Gran	BG12JV01	1.87	0.75638	0.00008	2.21	0.69693
	Gran	BG12JV01BIS	1.87	0.75697	0.00010	2.43	0.69752
	Gran	BG12JV02	1.87	0.76413	0.00010	0.95	0.69883
	Extr	BG12JV03	1.87	0.72925	0.00008	0.91	0.70260
	Extr	BG12JV07	1.87	0.72847	0.00007	0.60	0.70280
	Extr	BG12JV08	1.87	0.72014	0.00007	9.7	0.70329
	Extr	BG12JV09	1.87	0.84654	0.00011	0.53	0.57533
	Extr	BG12JV10	1.87	0.71886	0.00011	8.6	0.70409
	Gran	BG12JV12	1.96	0.96578	0.00013	14.0	0.72339
	Migm	BG12JV13	1.96	1.01188	0.00014	14.9	0.61986
	Gran	BG12JV18	1.96	1.16328	0.00016	0.49	0.77712
	Maf	IR12JV04	1.96	0.71787	0.00009	0.032	0.70398
	Maf	IR12JV05	1.96	0.72535	0.00008	25.0	0.72446
	Gran	IR12JV06	1.00	1.01064	0.00009	11.0	0.30984
	Gran	IR12JV13	1.00	0.98898	0.00020	0.93	0.68044
	Gran	IR12JV14	2.74	0.73393	0.00010	13.3	0.69709
Metasediments	Sed	BG12JV06	1.8	0.96556	0.00013	12.5	0.69883
	Sed	BG12JV14	1.8	0.93231	0.00012	7.6	0.62214
	Sed	BG12JV15	1.8	0.82021	0.00022	44.1	0.60987
	Sed	BG12JV17	1.8	1.46061	0.00022	8.4	0.62305
	Sed	IR12JV02	1.8	0.89840	0.00014	8.8	0.31947
	Sed	IR12JV03	1.8	0.86603	0.00014	2.99	0.68027
	Sed	IR12JV09	1.8	0.76562	0.00010	11.8	0.63873
	Sed	IR12JV10	1.8	0.97165	0.00011	2.21	0.68830

[a] The chosen age T for the undated Domes units is 1.92 Ga, the central value of the igneous Domes ages referenced in the text (1.98-1.86 Ga). This corresponds closely to the 1.91 Ga modus of igeous zircon ages by Eglinger (2013). Bangweulu and Irumide ages follow the central values from the corresponding magmatic phase of De Waele et al. (2006b) and references therein. The isotope composition of the Muva Supergroup and inferred correlatives is shown at the inferred depositional age of the former (~1.8 Ga, De Waele and Fitzsimons, 2007). [b] N.A., not applicable.

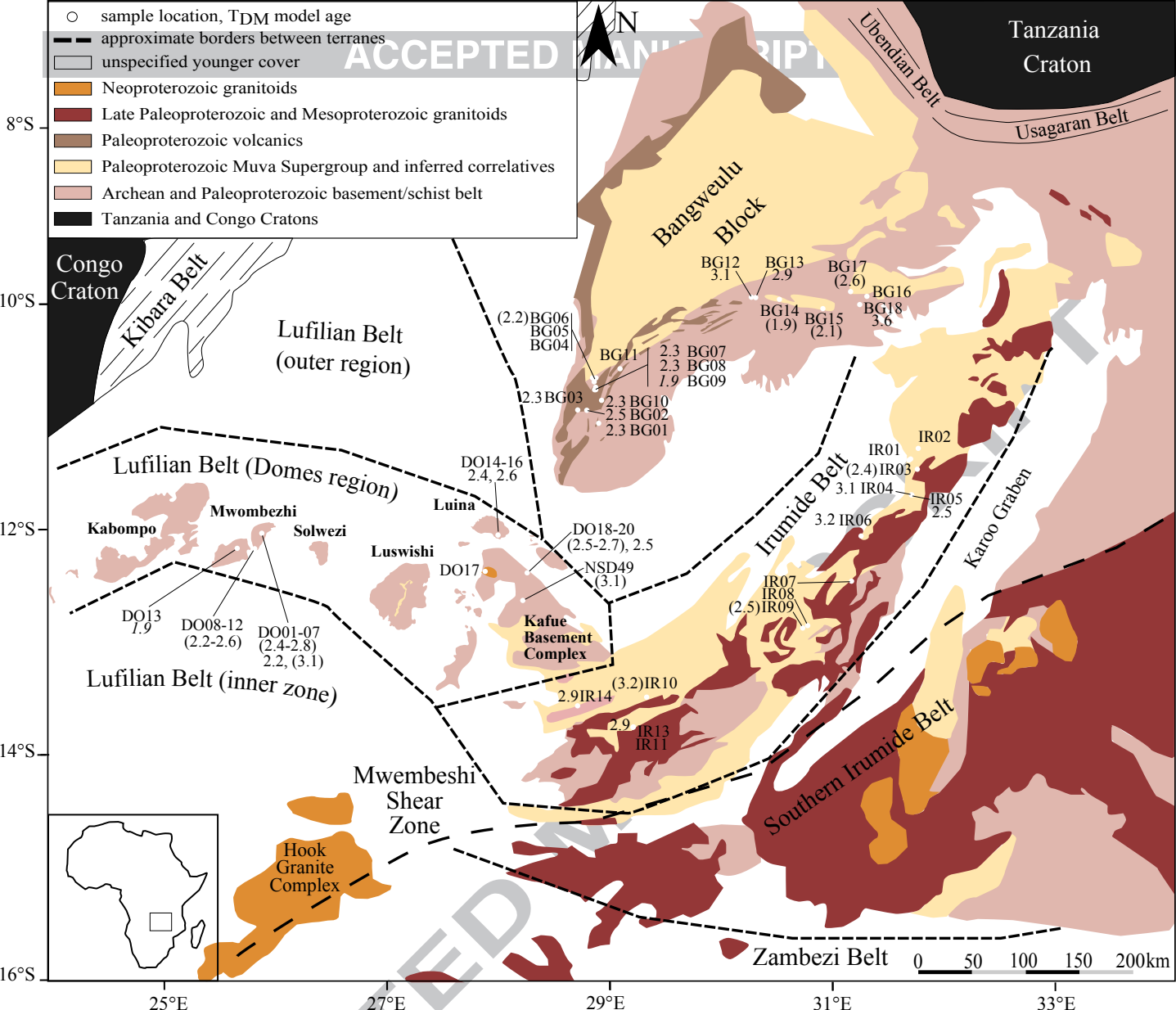
sample location, T_{DM} model age
approximate borders between terranes
unspecified younger cover
Neoproterozoic granitoids
Late Paleoproterozoic and Mesoproterozoic granitoids
Paleoproterozoic volcanics
Paleoproterozoic Muva Supergroup and inferred correlatives
Archean and Paleoproterozoic basement/schist belt
Tanzania and Congo Cratons
N
Tanzania Craton
Ubendian Belt
Usagaran Belt
Bangweulu Block
Congo Craton
Kibara Belt
Lufilian Belt (outer region)
Lufilian Belt (Domes region)
Lufilian Belt (inner zone)
Kabompo
Mwombezhi
Solwezi
Luswishi
Luina
Kafue Basement Complex
Irumide Belt
Karoo Graben
Southern Irumide Belt
Mwembeshi Shear Zone
Hook Granite Complex
Zambezi Belt
BG12 3.1
BG13 2.9
BG17 (2.6)
BG16
BG18 3.6
BG14 (1.9)
BG15 (2.1)
(2.2) BG06
BG05
BG04
BG11
2.3 BG07
2.3 BG08
1.9 BG09
2.3 BG03
2.3 BG10
2.5 BG02
2.3 BG01
DO14-16 2.4, 2.6
DO18-20 (2.5-2.7), 2.5
DO17
NSD49 (3.1)
DO13 1.9
DO08-12 (2.2-2.6)
DO01-07 (2.4-2.8) 2.2, (3.1)
IR02
IR01
(2.4) IR03
3.1 IR04
IR05 2.5
3.2 IR06
IR07
IR08
(2.5) IR09
(3.2) IR10
2.9 IR14
2.9 IR13
IR11
8°S
10°S
12°S
14°S
16°S
25°E
27°E
29°E
31°E
33°E
0 50 100 150 200km

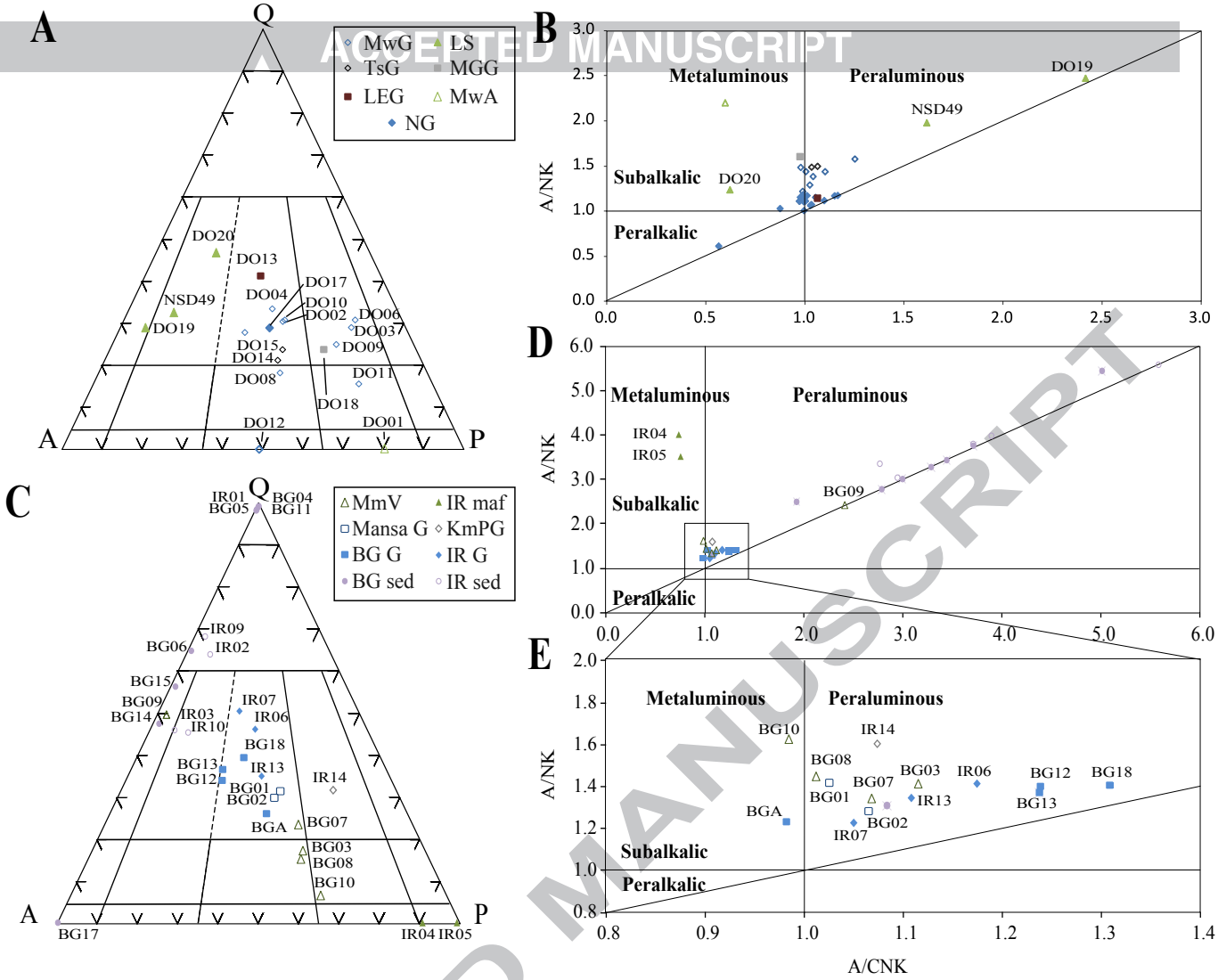

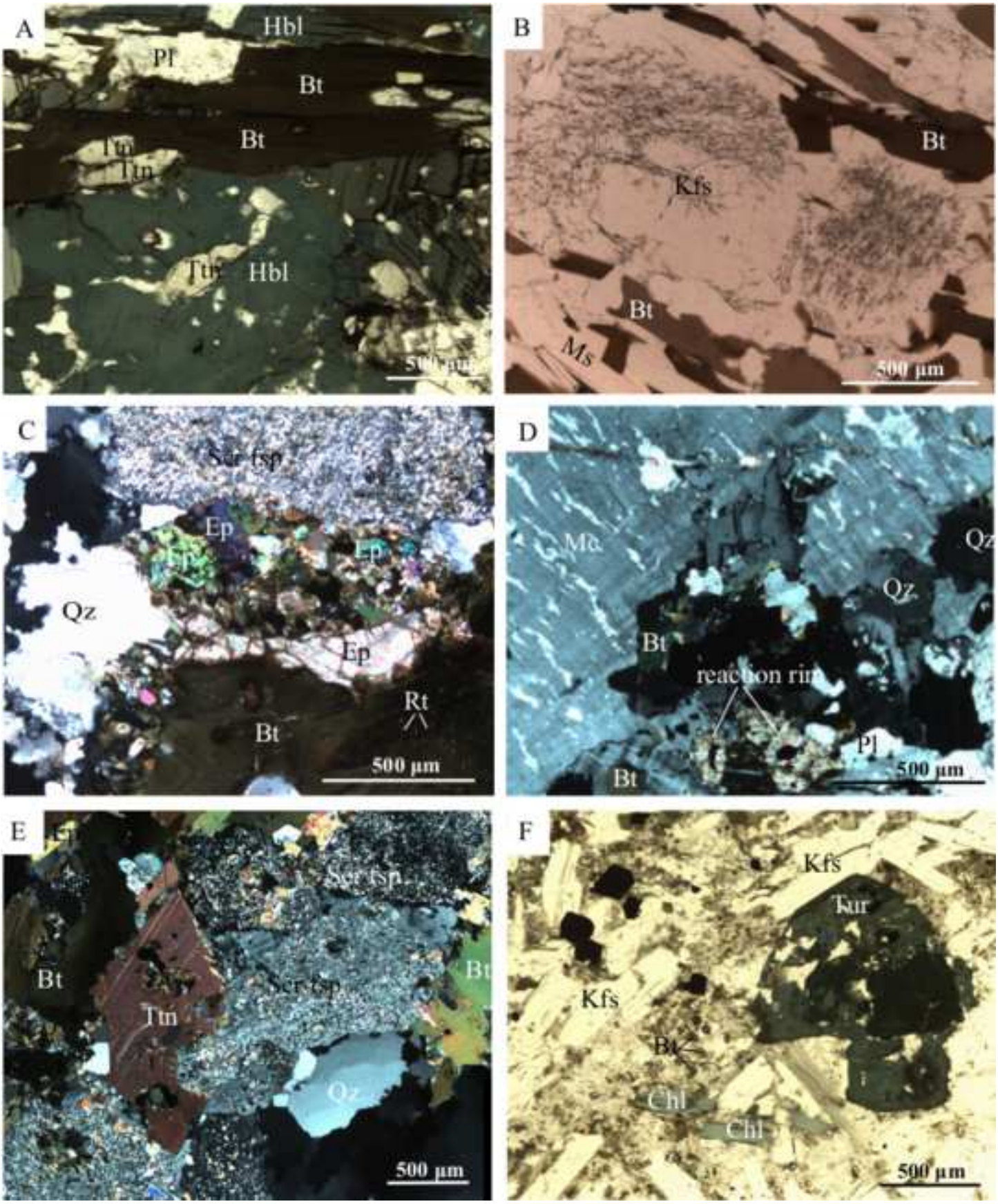

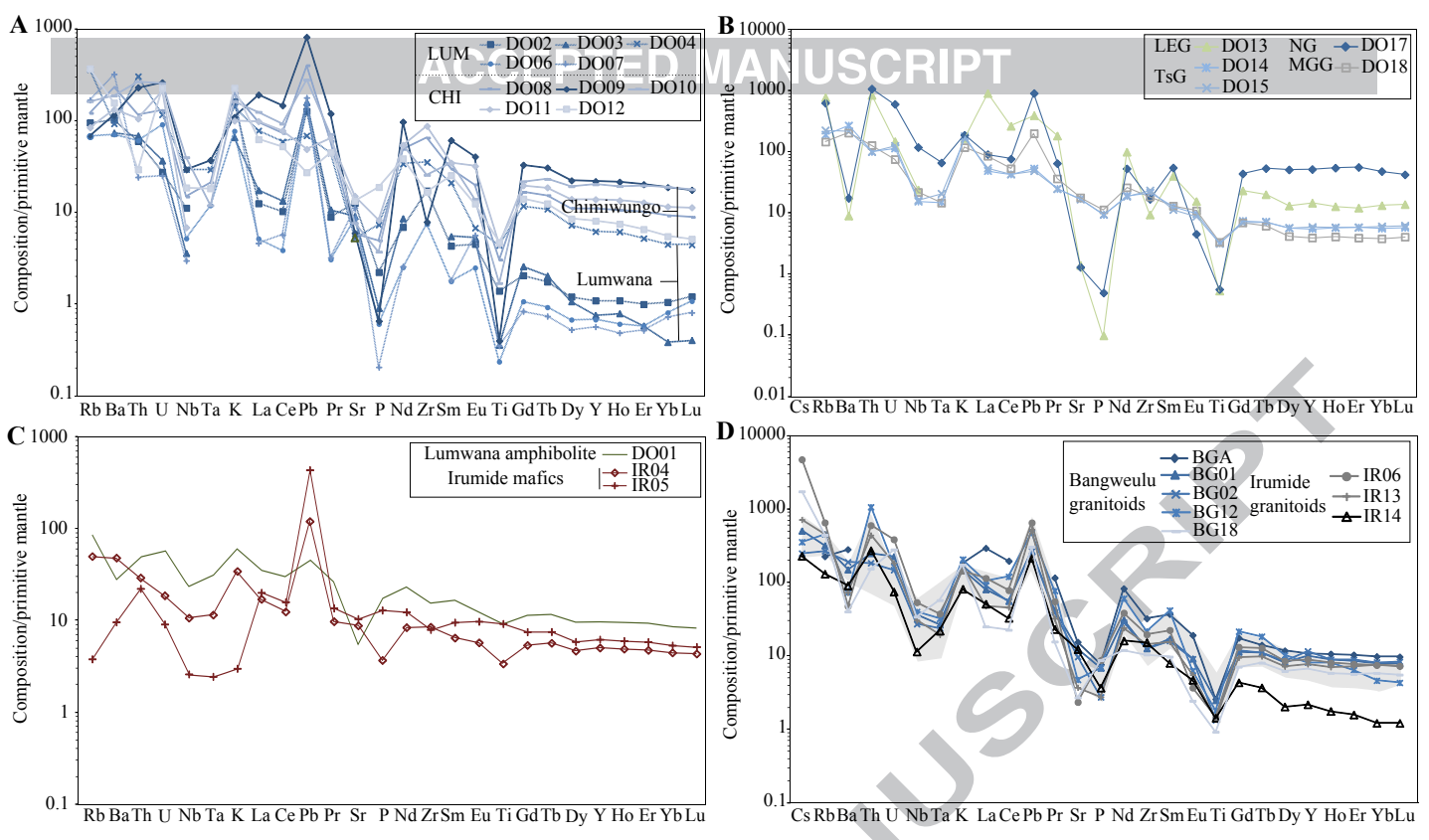
A
Composition/primitive mantle
LUM
DO02
DO03
DO04
DO06
DO07
CHI
DO08
DO09
DO10
DO11
DO12
Chimiwungo
Lumwana
Rb Ba Th U Nb Ta K La Ce Pb Pr Sr P Nd Zr Sm Eu Ti Gd Tb Dy Y Ho Er Yb Lu
B
LEG
DO13
NG
DO17
TsG
DO14
MGG
DO18
DO15
Cs Rb Ba Th U Nb Ta K La Ce Pb Pr Sr P Nd Zr Sm Eu Ti Gd Tb Dy Y Ho Er Yb Lu
C
Lumwana amphibolite
DO01
Irumide mafics
IR04
IR05
D
Bangweulu granitoids
BGA
BG01
BG02
BG12
BG18
Irumide granitoids
IR06
IR13
IR14

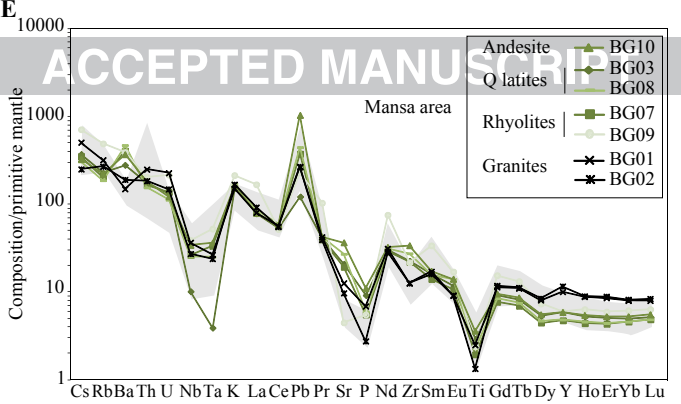

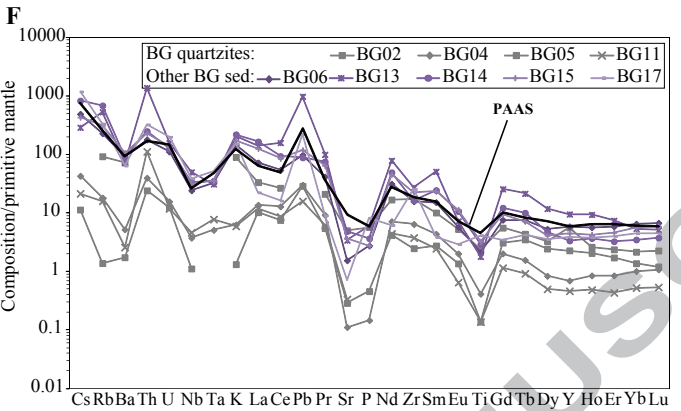

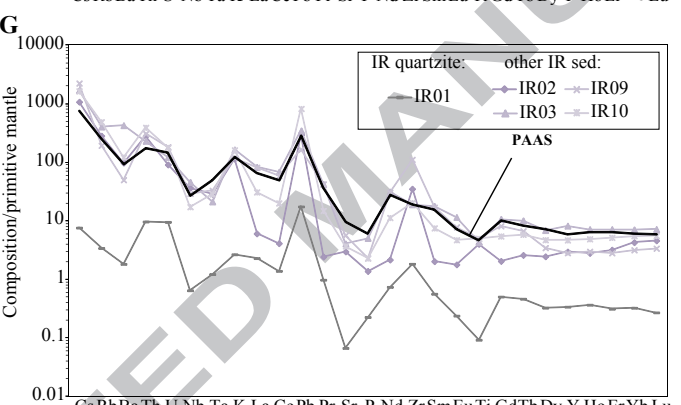

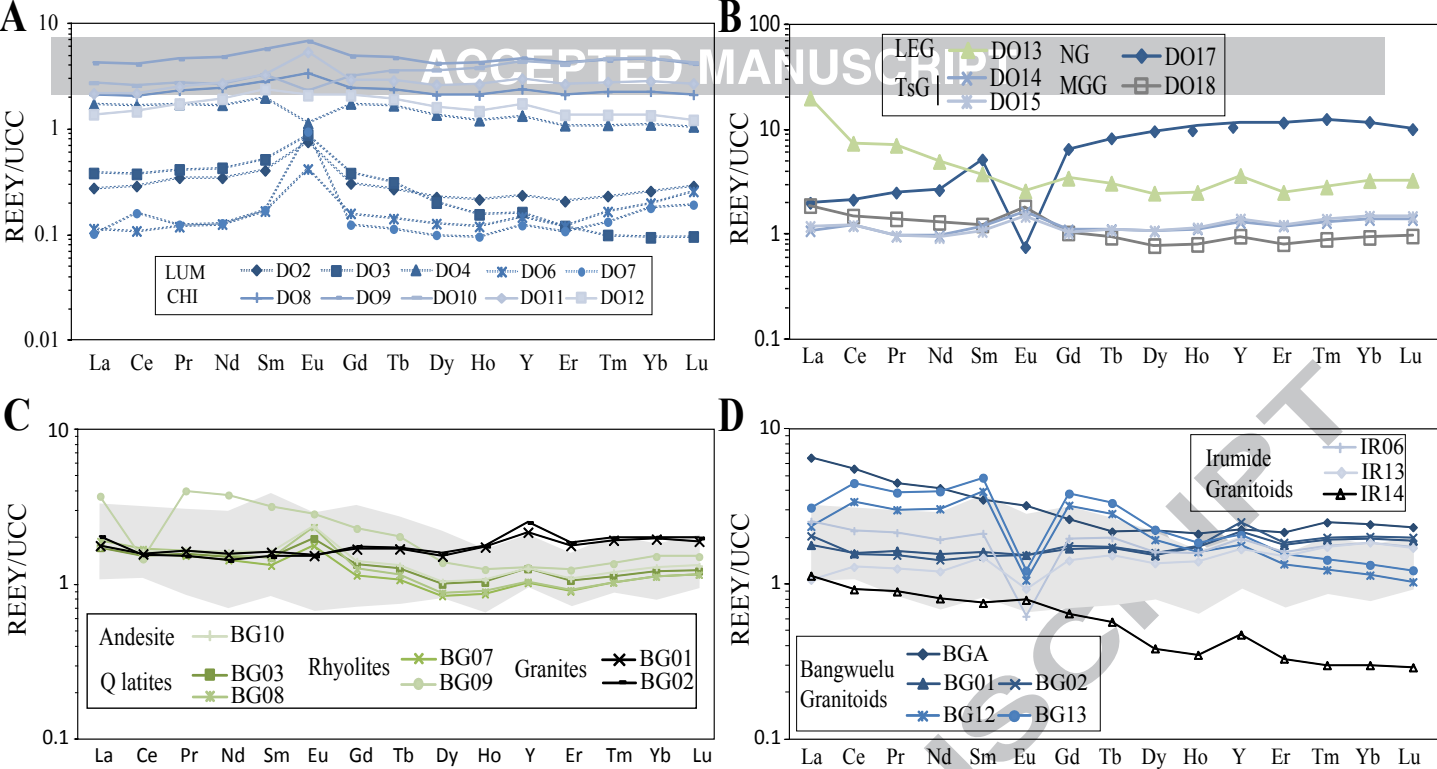

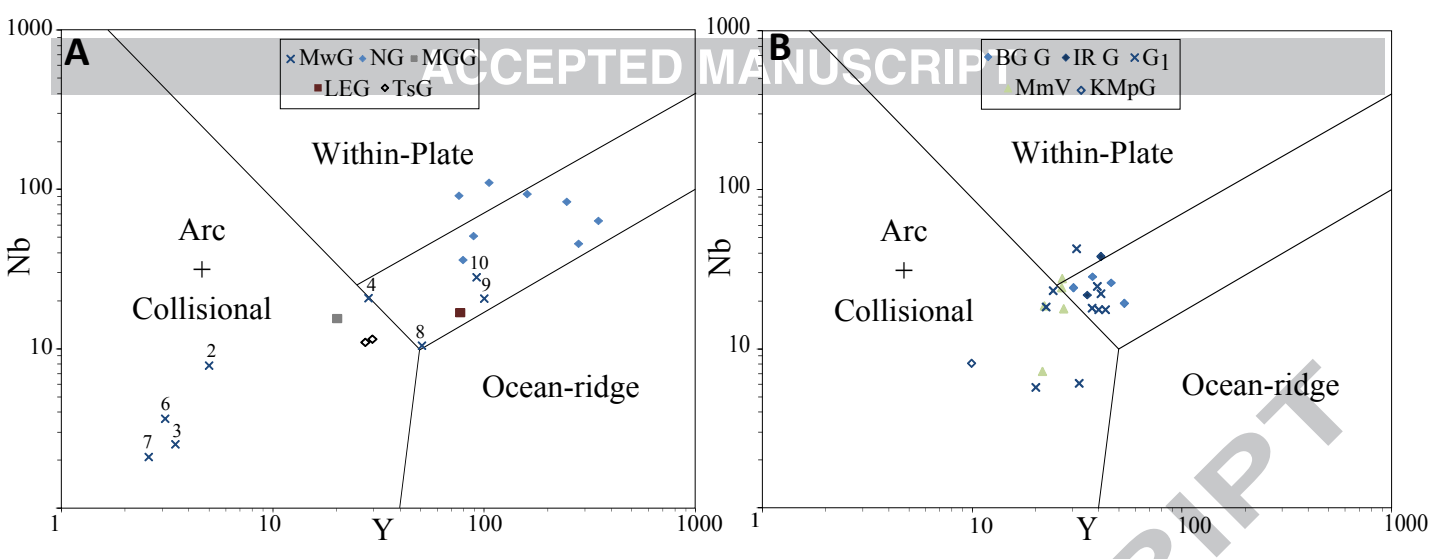

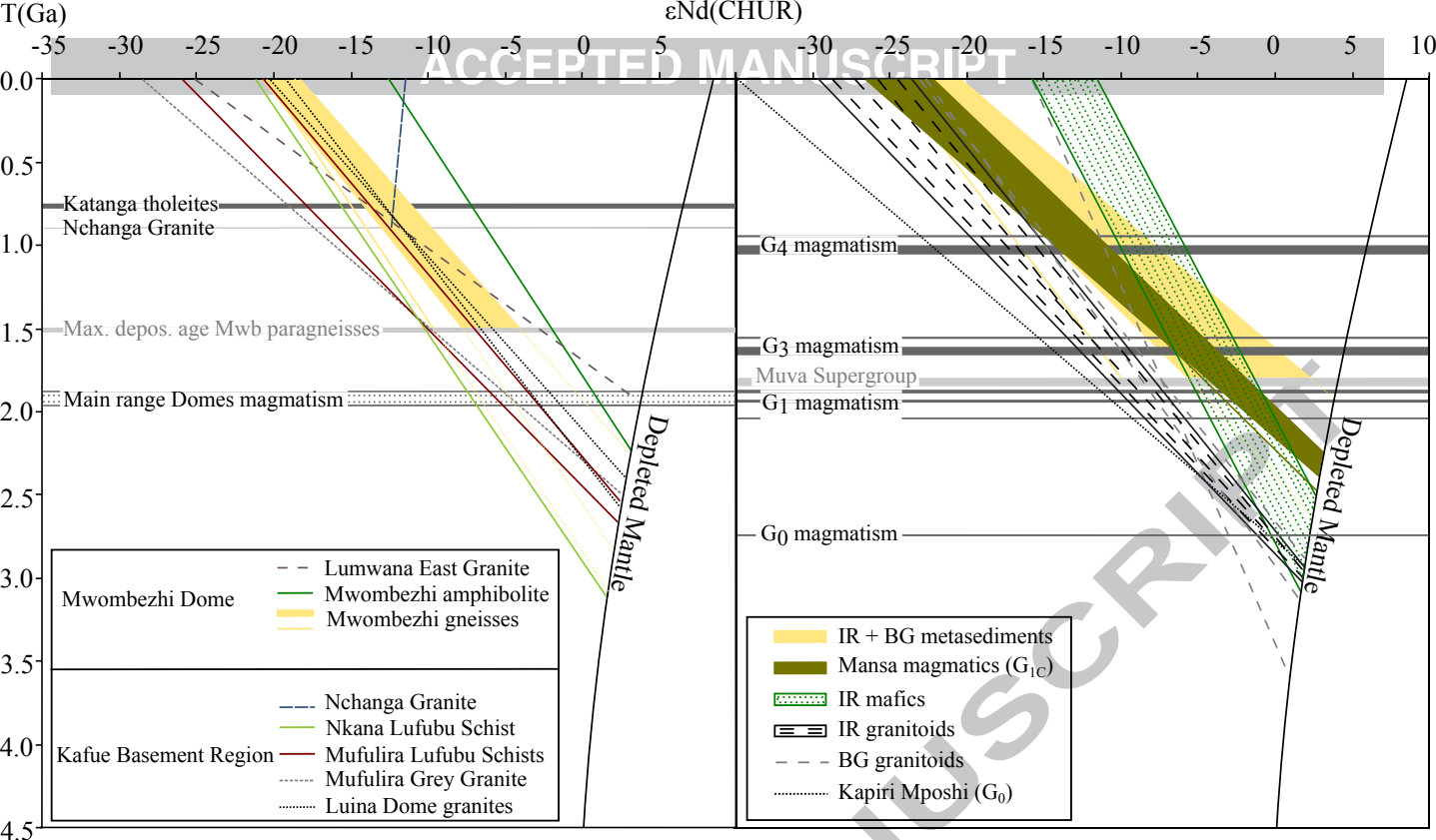

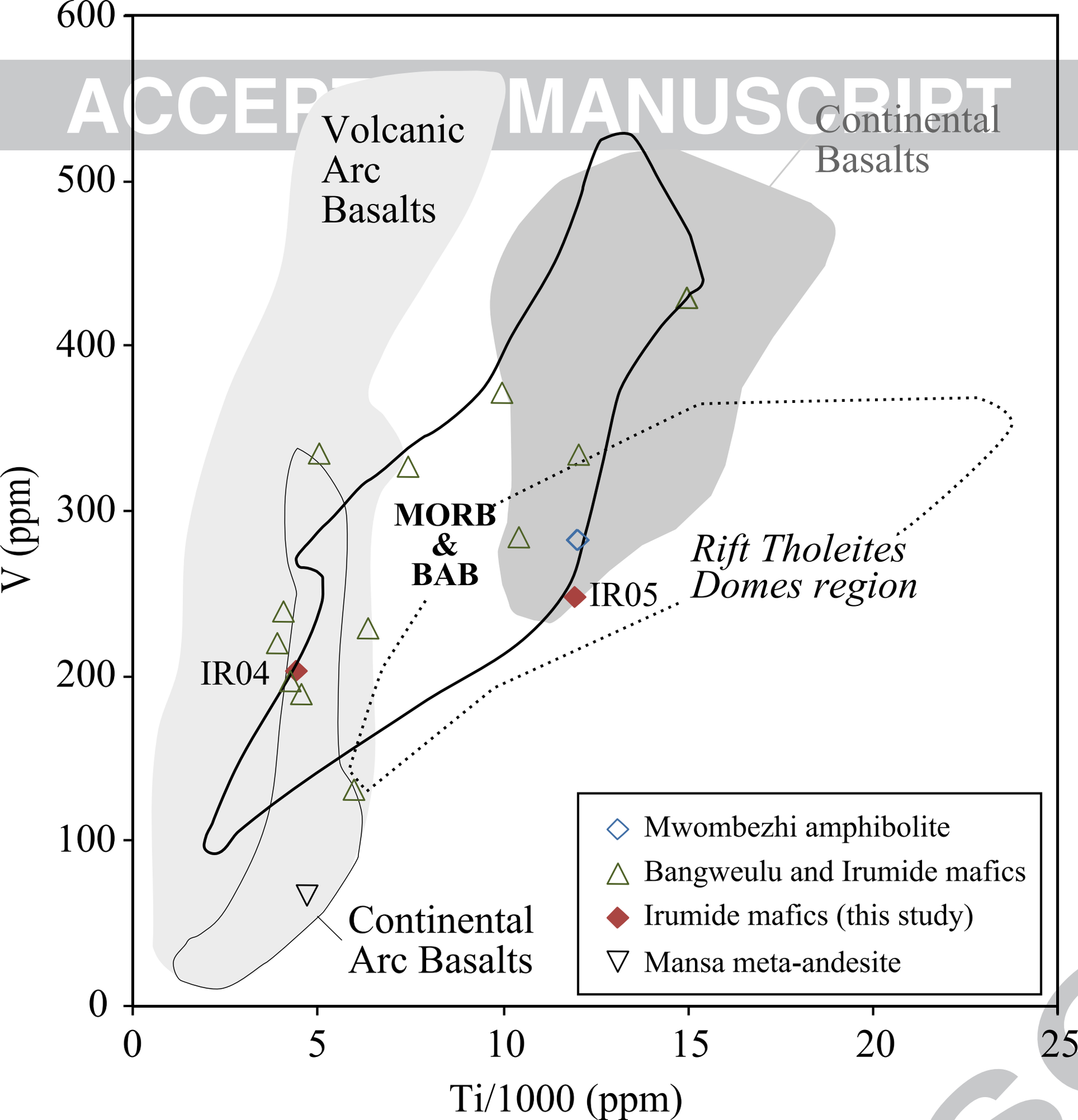

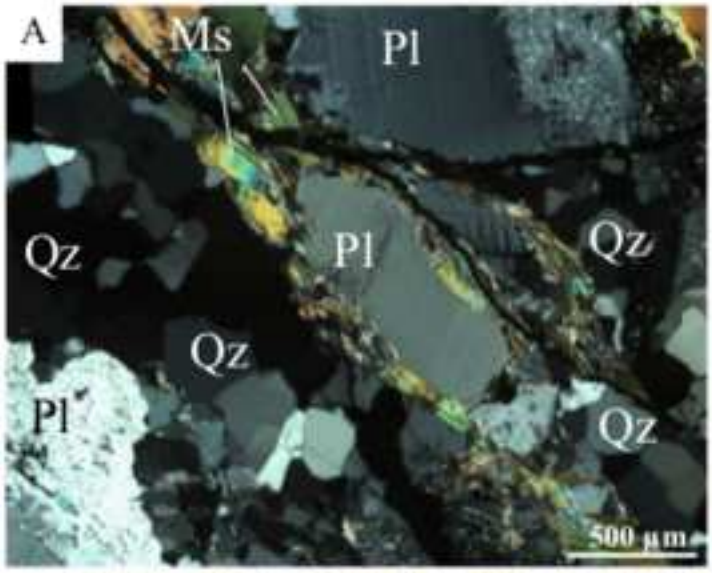

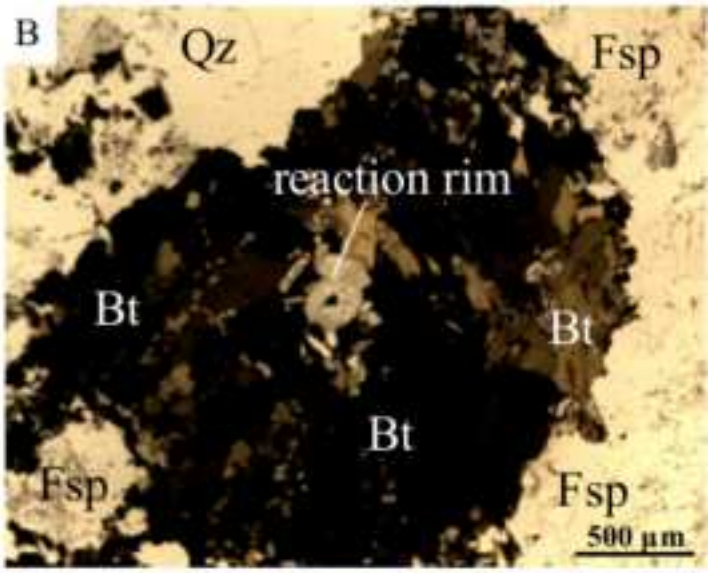

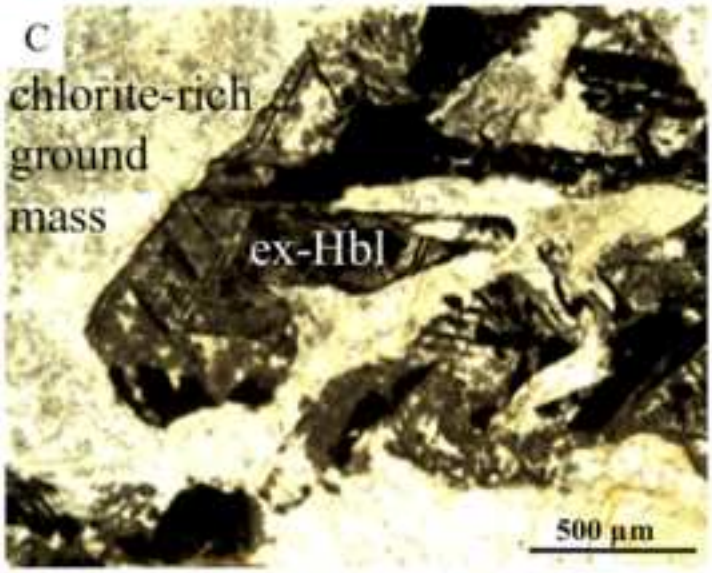

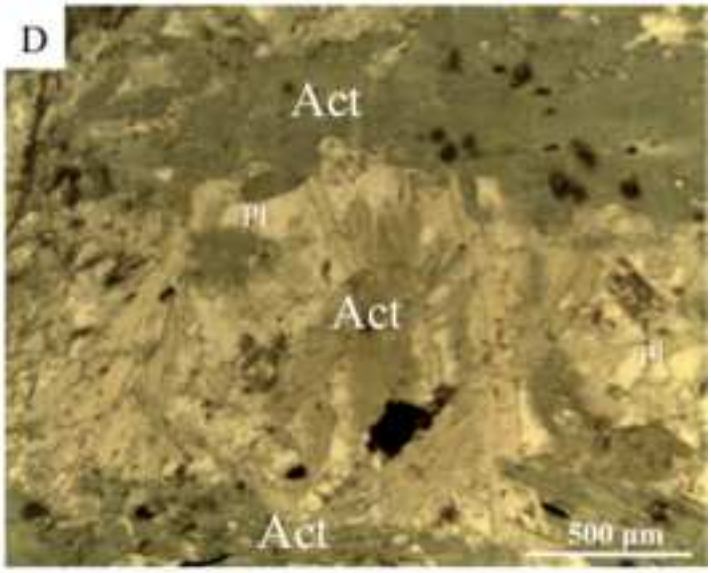

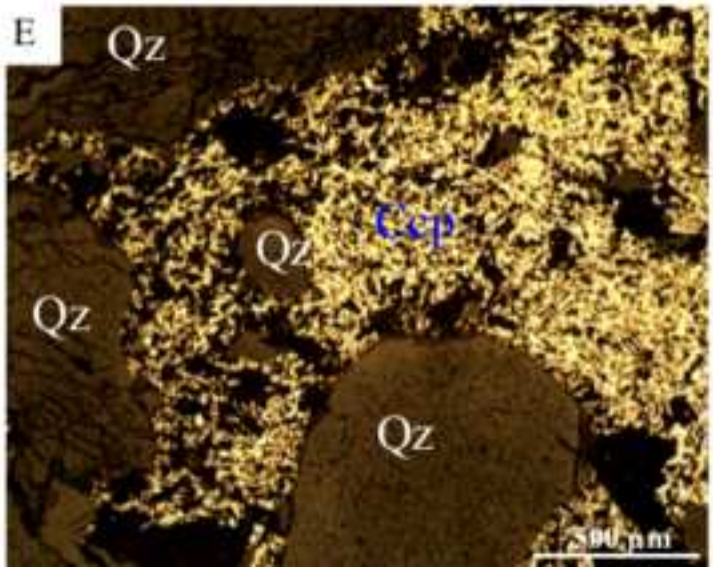

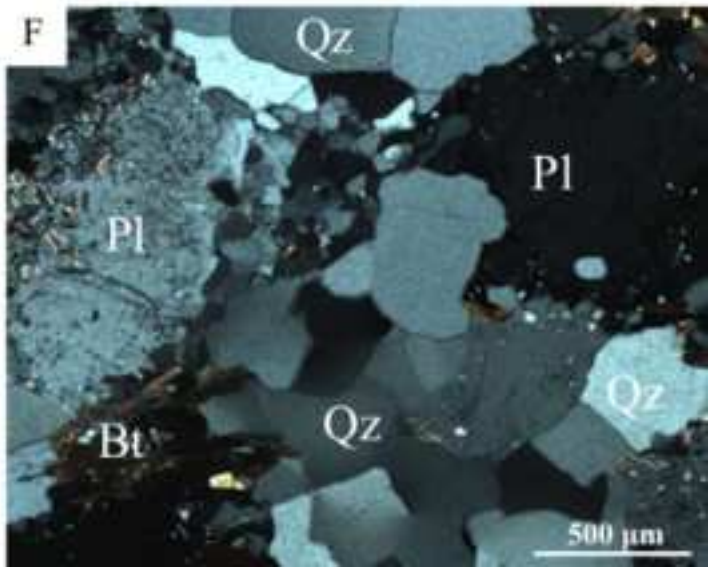

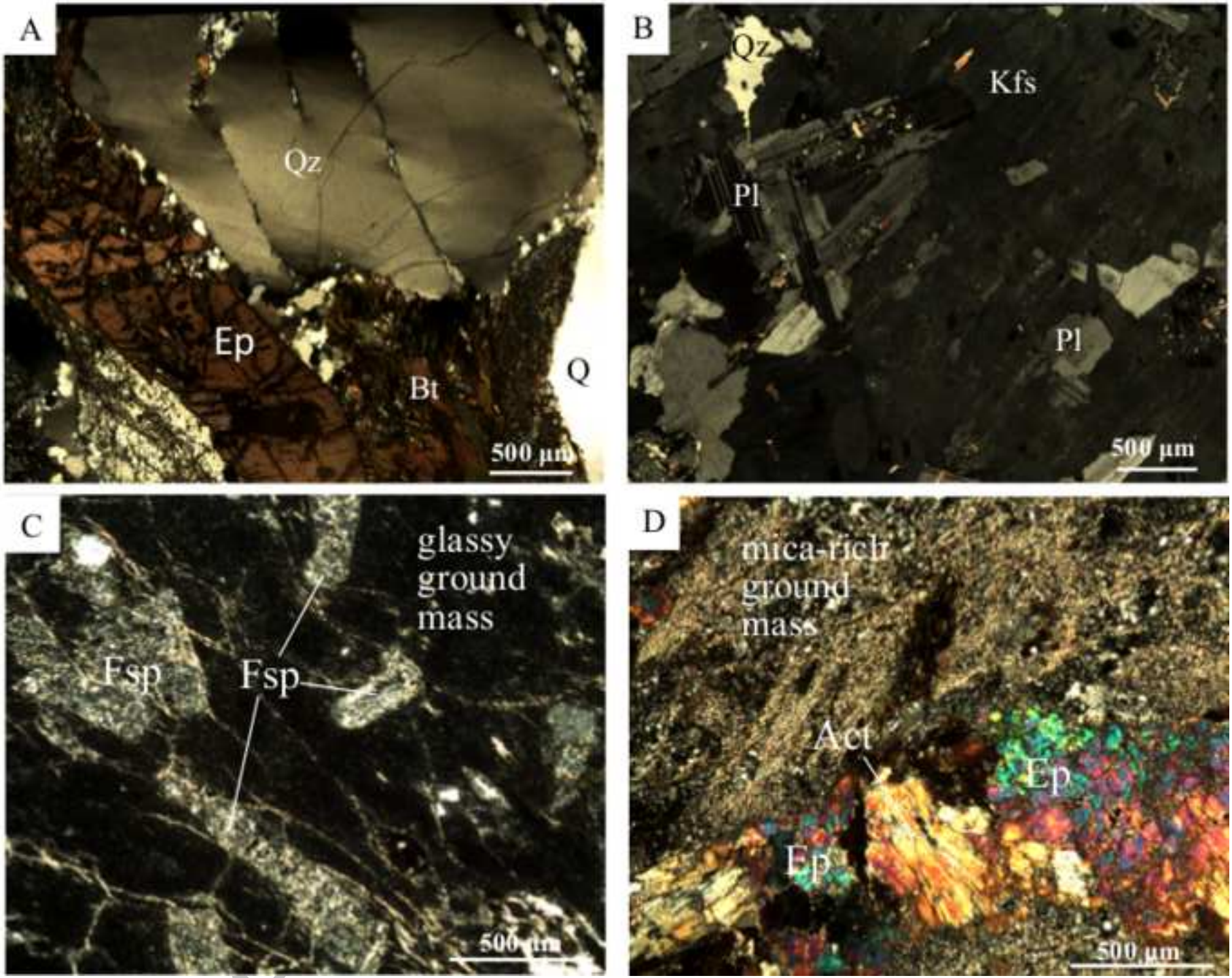

- Petrochemical and isotopic characterization of Domes, Irumide and Bangweulu units.
- Calculation of depleted mantle Nd model ages with analytically induced errors.
- Nd model ages reveal cryptic Archean sources in all terranes.
- The isotope data indicates long-lived crustal reworking in the entire region.
- Evidence for a Paleoproterozoic continental arc in the East Domes and SW Bangweulu.